

Review

A Review of Hyperon Physics at BESIII Experiment

Ruoyu Zhang  **Xiongfei Wang** *

¹ School of Physical Science and Technology, Lanzhou University, Lanzhou 730000, China; zhangry18@lzu.edu.cn

² Lanzhou Center for Theoretical Physics, Key Laboratory of Theoretical Physics of Gansu Province, Key Laboratory of Quantum Theory and Applications of MoE, Gansu Provincial Research Center for Basic Disciplines of Quantum Physics, Lanzhou University, Lanzhou 730000, China

³ Frontiers Science Center for Rare Isotopes, Lanzhou University, Lanzhou 730000, China

* Correspondence: wangxiongfei@lzu.edu.cn

Abstract

The BESIII Collaboration has collected large data samples from e^+e^- collisions at center-of-mass energies ranging from 1.84 to 4.95 GeV, which include the world's largest charmonium sample, consisting of 10 billion J/ψ and 3 billion $\psi(3686)$ events. These high-statistics datasets enable BESIII to carry out a wide range of studies in hyperon physics. In this article, we review the major achievements of the BESIII Collaboration in this field, which can be broadly categorized into four areas: hyperon polarization and CP violation, rare hyperon decays, hyperon pair production, and hyperon–nucleon interactions.

Keywords: CP violation; electromagnetic form factors; charmonium(-like) states; hyperon–nucleon scattering

1. Introduction

The Big Bang implies the production of equal amounts of matter and antimatter, which should have led to their complete annihilation in the early Universe [1]. However, observations indicate that the present Universe is overwhelmingly composed of matter, with little evidence of antimatter. This discrepancy has puzzled the scientific community for more than half a century and remains a subject of intensive research. One of the long-standing explanations is baryogenesis [2], in which the matter abundance is generated dynamically. A crucial requirement for its realization is the violation of charge-conjugation and parity (CP) symmetry. Therefore, exploring CP violation has become one of the key objectives of modern collider experiments. To date, the clear existence of CP violation has been established in weak interactions involving kaon, charm, and beauty meson decays [3–6]. There is also experimental evidence for CP violation in neutrino oscillations [7]. The observed CP violation in meson decays is well-interpreted by the Cabibbo–Kobayashi–Maskawa (CKM) mechanism [8,9]. However, the matter–antimatter asymmetry generated by the CKM mechanism is far too small to account for astronomical observations, posing a serious challenge to the Standard Model (SM) and indicating the possible existence of additional sources of CP violation [1]. This has driven the expansion of CP violation research into broader domains. Very recently, LHCb reported the first observation of CP violation in Λ_b^0 baryons [10], opening a new avenue in the search for physics beyond the SM. The development of angular distribution analysis based on the helicity formalism has provided a new approach to exploring CP violation in hyperons. The data samples of 10 billion J/ψ and 3 billion $\psi(3686)$ events collected by BESIII in e^+e^- collisions at center-of-mass (c.m.)



Academic Editor: Stefano Profumo

Received: 18 December 2025

Revised: 15 January 2026

Accepted: 19 January 2026

Published: 21 January 2026

Copyright: © 2026 by the authors.

Licensee MDPI, Basel, Switzerland.

This article is an open access article distributed under the terms and conditions of the [Creative Commons Attribution \(CC BY\) license](#).

energies (\sqrt{s}) of 3.097 and 3.686 GeV, respectively, are well-suited for hyperon CP tests, and both states exhibit sizable branching fractions to hyperon–antihyperon pairs. Moreover, e^+e^- annihilation offers an experimental environment with a relatively low background and enables the production of quantum-entangled hyperon pairs. These features create highly favorable conditions for studying hyperon CP violation at BESIII [11]. Furthermore, angular distribution analysis not only enables the exploration of CP violation but also provides a novel approach for accurately extracting hyperon form factors. Since the first experimental determination of the proton form factors in the 1950s [12], form factors have remained a fundamental property of baryons and have been extensively studied to this day. The angular distribution analysis allows the extraction of the modulus ratio of the form factors, thereby extending the study of form factors beyond the relatively stable proton and neutron and providing valuable insights into the internal structure of hyperons. In this respect, BESIII data collected at three energy regions, such as near the hyperon–antihyperon production threshold (2.396–2.900 GeV), around the $\psi(3686)$ resonance (3.68–3.71 GeV), and at the $\psi(3770)$ resonance (3.773 GeV), are used in the analyses.

Another way to probe physics beyond the SM is through searches for rare decays, including in the hyperon sector. Within and beyond the SM, many theoretical models predict baryon-number-violating (BNV) decays. Experimentally, extensive searches have been carried out, but no evidence for such processes has been observed so far. Among the theories, some predict BNV decays that obey $\Delta(B - L) = 0$, where $\Delta(B - L)$ denotes the change in the difference between baryon and lepton numbers. As a hyperon factory, BESIII provides an opportunity to explore BNV decays in hyperons, while the presence of an s quark coupled to a u or d quark in hyperons allows the study of possible interference among multiple amplitudes in BNV transitions, an effect that has not been taken into account in existing theoretical calculations due to the ample parameter space. On the other hand, hyperon semileptonic decays provide valuable insight into the interplay between strong and weak interactions. The $\Delta S = \Delta Q$ rule is a fundamental assumption arising from the SU(3) symmetry of the weak hadronic current in the Cabibbo theory of weak interactions, introduced to explain the experimental absence of certain hyperon decay modes. Here, ΔS and ΔQ denote the changes in strangeness and charge between the initial and final state hadrons, respectively. Searching for hyperon semileptonic decays that violate the $\Delta S = \Delta Q$ rule would, therefore, signal the presence of weak currents associated with higher SU(3) multiplets. To ensure sufficient statistics, the full data sample of J/ψ data collected by BESIII is used in these studies.

At BESIII, substantial data samples have also been collected from the hyperon pair production threshold up to the energy region of the XYZ states [13], ranging from 1.84 to 4.95 GeV, providing valuable opportunities to study hyperon pair production in e^+e^- annihilation, to further explore the nature of charmonium(-like) states, and to test the nonperturbative theory of quantum chromodynamics. Experimental observations of the vector charmonium(-like) states exceed the predictions of potential models. This difference provide a significant opportunity to probe exotic configurations of quarks and gluons [14]. A variety of theoretical interpretations, including hybrid, multiquark, and molecular configurations [15–21], have been proposed to explain charmonium(-like) states. Nevertheless, no definitive conclusion has been reached, and the underlying nature of these states remains unresolved. This situation highlights our incomplete understanding of strong interaction dynamics in the nonperturbative regime. Further progress therefore relies on more precise experimental measurements. In this context, investigations of hyperon decays of charmonium(-like) states are particularly attractive, owing to their simple final state topologies and comparatively well-understood decay mechanisms. Additionally, the discovery of charmonium(-like) states in e^+e^- annihilation into charmonium and light

hadrons highlights the importance of studying hyperon final states, where information is still limited [22].

In addition, scattering experiments play a central role in probing the fundamental forces and internal structure of matter. Over the years, various types of particle beams have been produced and applied in scattering experiments, driving numerous scientific breakthroughs. However, for other neutral particles that are experimentally difficult to control, as well as long-lived hyperons and their antiparticles, experimental measurements remain scarce, even though they possess considerable physical potential. As a result, precise modeling of hyperon–nucleon and hyperon–hyperon interactions remains difficult, despite the availability of strong constraints and well-established descriptions for nucleon–nucleon interactions [23,24]. The properties of hyperons in dense matter have therefore drawn significant attention, owing to their close relevance to hypernuclei and to the role of hyperons in neutron stars [25]. In neutron stars, the possible presence of hyperons decreases the Fermi pressure of the system in the equation of state (EoS), thereby reducing the maximum mass that a neutron star can sustain. EoS calculations that include hyperons often predict a maximum mass lower than the observed values—a discrepancy known as the “hyperon puzzle” [26–28], which further motivates the exploration of hyperon–nucleon interactions. Based on the abundant hyperon data produced in J/ψ decays, BESIII has pioneered a series of hyperon–nucleon scattering studies using the nucleons in the beam-pipe material as targets.

In this article, we review recent results from the BESIII experiment related to hyperon polarization and CP violation, rare hyperon decays, hyperon production cross sections, and studies of hyperon–nucleon scattering.

2. The BESIII Detector

The BESIII detector [29] has recorded data from symmetric electron–positron collisions provided by the BEPCII storage ring [30], covering c.m. energies from 1.84 to 4.95 GeV. At $\sqrt{s} = 3.773$ GeV, it achieved a peak luminosity of $1.1 \times 10^{33} \text{ cm}^{-2}\text{s}^{-1}$. BESIII has accumulated a large data sample in this energy region [31–33].

The cylindrical core of the Beijing Spectrometer III (BESIII) detector covers 93% of the solid angle and consists of a helium-based multi-wire drift chamber (MDC), a time-of-flight (TOF) detector, and a CsI(Tl) electromagnetic calorimeter (EMC). These detecting components are housed within a superconducting solenoid magnet that provides a magnetic field of 1.0 Tesla (0.9 Tesla in 2012). The solenoid is supported by an octagonal yoke, which incorporates resistive plate chambers for muon identification interleaved with steel plates. The detection efficiency for charged particles and photons within a 4π solid angle is 93%. At a momentum of $1 \text{ GeV}/c$, the momentum resolution for charged particles is 0.5%, and for electrons from Bhabha scattering, the dE/dx resolution is 6%. The EMC achieves an energy resolution of 2.5% (5%) for 1 GeV photons in the barrel (end-cap) region. The plastic scintillator TOF detector has a time resolution of 68 ps in the barrel, while it was originally 110 ps in the end-cap region. The end-cap system was upgraded in 2015 using multi-gap resistive plate chamber technology, improving the time resolution to 60 ps and effectively enhancing data quality [34–36].

3. Hyperon Polarization and CP Violation

3.1. Analysis Method

The CP asymmetry is usually probed by comparing the decay patterns of a particle and its antiparticle. At BESIII, it is studied through angular distribution analysis within the helicity formalism, using decay parameters as observables. The interaction vertex of

quantum-entangled spin-1/2 hyperon–antihyperon pairs produced via e^+e^- annihilation can be described by two electromagnetic form factors (EMFFs), G_M and G_E [37,38]:

$$\Gamma_\mu(p_1, p_2) = -ie_g \left[G_M \gamma^\mu - \frac{2M}{Q^2} (G_M - G_E) Q_\mu \right], \quad (1)$$

where M is the hyperon mass, p_1 and p_2 are the hyperon and antihyperon momenta, respectively, $Q = p_1 - p_2$, and e_g is the coupling strength. Based on this, the angular distribution can be characterized by two real parameters: one corresponding to the ratio of the absolute values of the EMFFs, and the other representing their relative phase:

$$\begin{aligned} \alpha_\psi &= \frac{s|G_M|^2 - 4M^2|G_E|^2}{s|G_M|^2 + 4M^2|G_E|^2}, \\ \frac{G_E}{G_M} &= e^{i\Delta\Phi} \left| \frac{G_E}{G_M} \right|. \end{aligned} \quad (2)$$

The production via charmonium states follows the same formalism, with the corresponding form factors, G_E^ψ and G_M^ψ , referred to as psionic form factors [38]. Based on the optical theorem, the form factors in the space-like region are real at the lowest order as a consequence of the Hermiticity of the electromagnetic Hamiltonian, whereas in the time-like region they become complex, giving rise to transverse polarization of the produced hyperons [39–41]. In general, by defining the coordinate system as shown in Figure 1, the polarization terms can be expressed as follows [42,43]:

$$P_y(\cos\theta) = \frac{\sqrt{1 - \alpha_\psi^2 \sin(\Delta\Phi) \cos\theta \sin\theta}}{1 + \alpha_\psi \cos^2\theta}, \quad (3)$$

while a projection variable $\mu(\cos\theta)$ (or $M(\cos\theta)$) is often defined experimentally to illustrate the model's description of data and reveal the polarization signal:

$$\mu(\cos\theta) = \frac{m}{N} \sum_{i=1}^{N_k} (n_{1,y}^{(i)} - n_{2,y}^{(i)}), \quad (4)$$

where m represents the bin number in $\cos\theta$, N is the total number of events in the data sample, N_k is the number of events in the k -th $\cos\theta$ bin, and $\hat{\mathbf{n}}_1$ ($\hat{\mathbf{n}}_2$) denotes the unit vector along the direction of the daughter (antidaugther) particle in the rest frame of the hyperon (antihyperon).

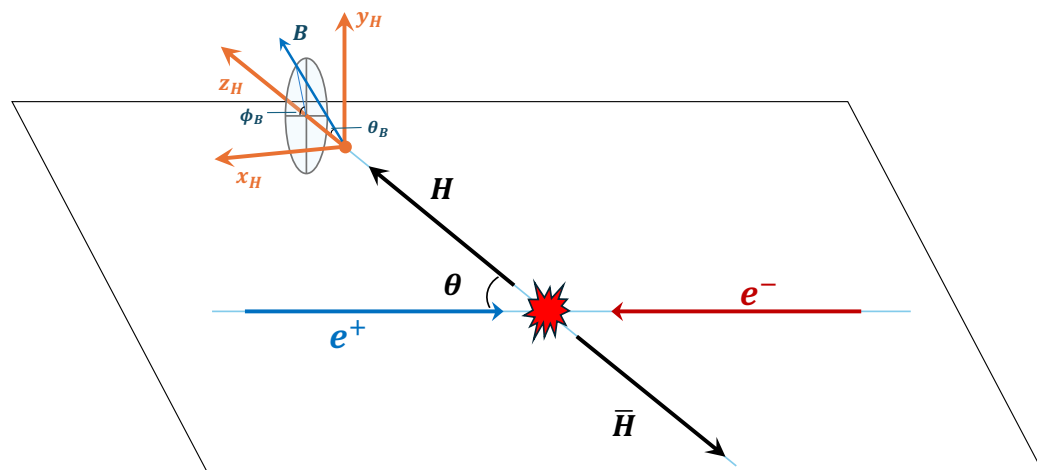


Figure 1. Orientation axes of the hyperon H and antihyperon \bar{H} helicity frames. B represents the baryon produced by H decay.

Subsequently, the decay amplitude of a spin-1/2 hyperon can be written as a combination of *S*-wave and *P*-wave contributions,

$$S = |S|e^{i(\delta_S + \xi_S)}, \quad (5)$$

$$P = |P|e^{i(\delta_P + \xi_P)},$$

where $\delta_{S(P)}$ and $\xi_{S(P)}$ denote the strong and weak phases, respectively. These amplitudes are associated with *CP* conservation and violation, and are characterized by the Lee–Yang parameters α_H , β_H , and γ_H [44], which satisfy the normalization condition $\alpha_H^2 + \beta_H^2 + \gamma_H^2 = 1$. They are further expressed by defining a parameter $\phi_H = \tan^{-1}(\beta_H/\gamma_H)$. If *CP* is conserved, the above hyperon decay parameters should be equal in magnitude but opposite in sign to those of their corresponding antiparticles. This allows us to define observables for *CP* violation:

$$A_{CP} = \frac{\alpha_H + \alpha_{\bar{H}}}{\alpha_H - \alpha_{\bar{H}}} = \frac{\beta_H + \beta_{\bar{H}}}{\beta_H - \beta_{\bar{H}}} = \frac{\gamma_H + \gamma_{\bar{H}}}{\gamma_H - \gamma_{\bar{H}}}, \quad (6)$$

$$\Delta\phi_{CP} = \frac{\phi_H + \phi_{\bar{H}}}{2}.$$

In addition, based on the strong ($\delta_P - \delta_S$) and weak ($\xi_P - \xi_S$) phase differences between the *S*-wave and *P*-wave, the *CP* violation observables can be further expressed as [45,46]

$$A_{CP} \approx -\tan(\delta_P - \delta_S) \tan(\xi_P - \xi_S). \quad (7)$$

3.2. Charmonium Decay

BESIII has recently reported a series of measurements on hyperon spin polarization, aiming to explore possible indications of *CP* violation. These measurements are based on the world's largest J/ψ and $\psi(3686)$ data samples. Due to differences in data-taking periods, some analyses were performed using only partial datasets. The most precise measurement of the Λ decay parameters was performed using the process $J/\psi \rightarrow \Lambda\bar{\Lambda}$ [47], as shown in Figure 2a. A clear polarization signal was observed, and the measurements of the decay parameters α_-^Λ for $\Lambda \rightarrow p\pi^-$ and $\alpha_+^{\bar{\Lambda}}$ for $\bar{\Lambda} \rightarrow \bar{p}\pi^+$ achieved the highest precision to date, with results of $\alpha_-^\Lambda = 0.7519 \pm 0.0036 \pm 0.0024$ and $\alpha_+^{\bar{\Lambda}} = -0.7559 \pm 0.0036 \pm 0.0030$, respectively. The *CP* violation observable for the Λ decay was determined to be $A_{CP}^- = 0.0025 \pm 0.0046 \pm 0.0012$, which is consistent with zero, indicating no evidence of *CP* violation. Meanwhile, the angular distribution parameters $\alpha_{J/\psi}$ and $\Delta\Phi$ are also determined to be $\alpha_{J/\psi} = 0.4748 \pm 0.0022 \pm 0.0031$ and $\Delta\Phi = 0.7521 \pm 0.0042 \pm 0.0066$ rad.

The isospin-violating process $J/\psi \rightarrow \Lambda\bar{\Sigma}^0$, together with its charge-conjugation (c.c.), can also be studied through joint angular distribution analysis [48]. The fit results of P_γ in each $\cos\theta_{\Sigma^0/\bar{\Sigma}^0}$ bin are shown in Figure 2a. Unlike hyperon–antihyperon pair production, non-charge-conjugated final states Λ and $\bar{\Sigma}^0$ enable exploration of direct *CP* violation by comparing the polarizations extracted from both decay modes. The measurement extracted $\alpha_{J/\psi} = 0.418 \pm 0.028 \pm 0.014$, $\Delta\Phi_{\bar{\Lambda}\Sigma^0} = 1.011 \pm 0.094 \pm 0.010$ rad, and $\Delta\Phi_{\Lambda\bar{\Sigma}^0} = 2.128 \pm 0.094 \pm 0.010$ rad. Furthermore, the modulus ratio of the form factors was determined to be $R = 0.860 \pm 0.029 \pm 0.015$, and the *CP* violation observable, $\Delta\Phi_{CP} = |\pi - (\Delta\Phi_{\bar{\Lambda}\Sigma^0} + \Delta\Phi_{\Lambda\bar{\Sigma}^0})| = 0.003 \pm 0.133 \pm 0.014$, is consistent with zero, indicating no significant evidence for direct *CP* violation.

For the $\Sigma^+\bar{\Sigma}^-$ hyperon pair, based on both the J/ψ and $\psi(3686)$ data samples, BESIII first reconstructed the decays via the dominant channels $\Sigma^+ \rightarrow p\pi^0$ and $\bar{\Sigma}^- \rightarrow \bar{p}\pi^0$, and measured their decay parameters [49,50]. Subsequently, by reconstructing one side of the decay through the neutron channel, the decay parameters of $\Sigma^+ \rightarrow n\pi^+$ and $\bar{\Sigma}^- \rightarrow \bar{n}\pi^-$ were measured [51], representing the first test of *CP* symmetry in hyperon decays involving

a neutron final state. The ratio of the decay asymmetry parameters for the two isospin decay modes serves as a sensitive probe for determining the contribution of $\Delta I = 3/2$ transitions and for investigating the $\Delta I = 1/2$ rule [52]. As observables, the ratios of the decay asymmetry parameters, $\alpha_+^{\Sigma^+}/\alpha_0^{\Sigma^+}$ and $\alpha_-^{\Sigma^-}/\alpha_0^{\Sigma^-}$, are found to be smaller than unity by more than 5σ , indicating the presence of a $\Delta I = 3/2$ transition.

The decay parameters of the radiative decay $\Sigma^0 \rightarrow \gamma\Lambda$ offer an opportunity to explore parity and strong CP violation beyond the SM [53]. In this case, the CP violation observable is defined as $A_{CP}^{\Sigma^0} = \alpha^{\Sigma^0} + \alpha^{\bar{\Sigma}^0}$. Based on both J/ψ and $\psi(3686)$ data samples, BESIII has also carried out a related study [54]. The aforementioned measurements of the Σ hyperons are summarized in Table 1, with results consistent with CP conservation. The observed polarization signals are shown in Figure 2b,c.

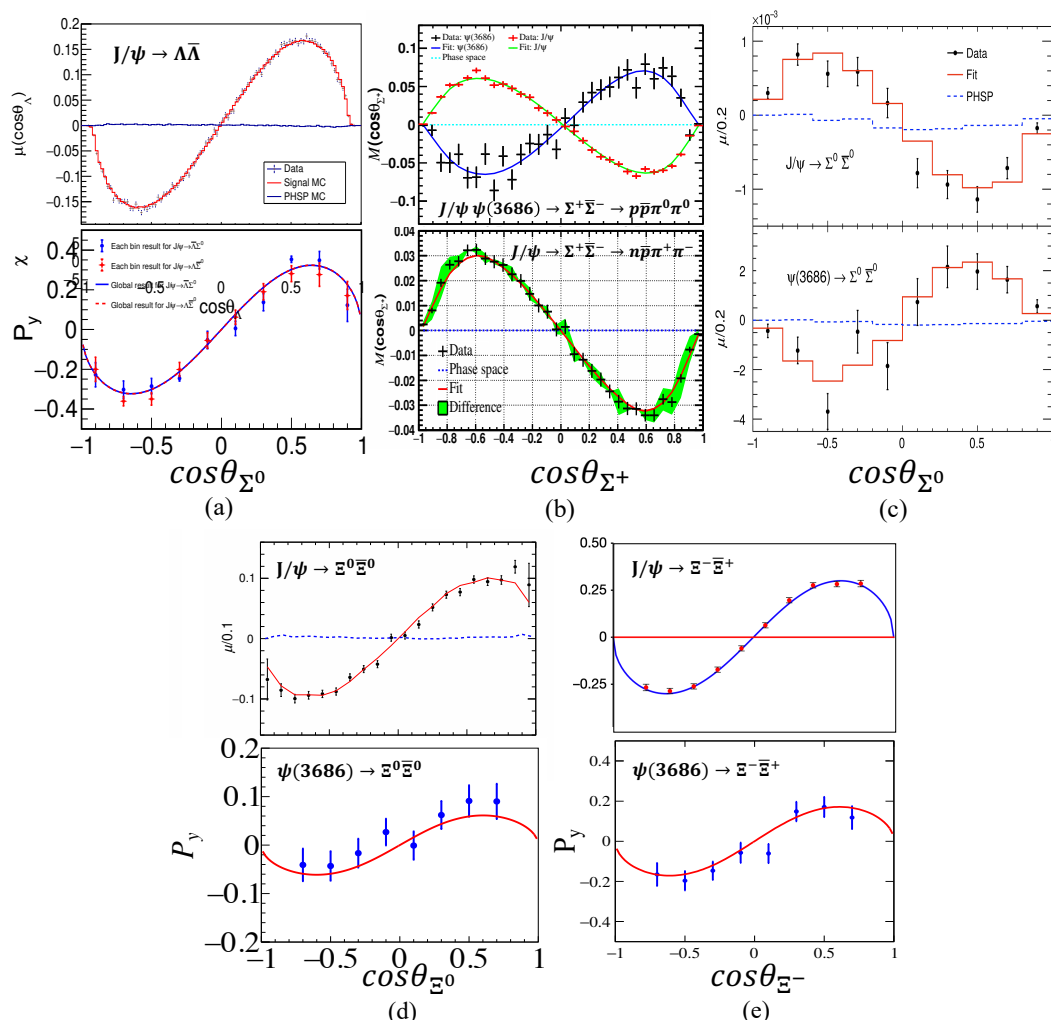


Figure 2. Distributions of the polarization observables μ for $J/\psi \rightarrow \Lambda\bar{\Lambda}$ [47] (a), $J/\psi/\psi(3686) \rightarrow \Sigma^0\bar{\Sigma}^0$ [54] (c), and $J/\psi \rightarrow \Xi^0\bar{\Xi}^0$ [55] (d); M for $J/\psi/\psi(3686) \rightarrow \Sigma^+\bar{\Sigma}^-$ [50,51] (b); and P_y for $J/\psi \rightarrow \Lambda\Sigma^0 + \text{c.c.}$ [48] (a), $\psi(3686) \rightarrow \Xi^0\bar{\Xi}^0$ [56] (d), and $J/\psi/\psi(3686) \rightarrow \Xi^-\bar{\Xi}^+$ [57,58] (e), as functions of $\cos\theta$ for each process. The dots with error bars represent the experimental data, the colored solid curves denote the global fit results, the dashed histograms correspond to the phase space (PHSP) Monte Carlo (MC) samples, and the red solid histograms show the PHSP MC weighted according to the global fit.

Table 1. Fitting results of each decay parameter for $J/\psi/\psi(3686) \rightarrow \Sigma^+\bar{\Sigma}^-$ and $J/\psi/\psi(3686) \rightarrow \Sigma^0\bar{\Sigma}^0$. The first uncertainty is statistical and the second is systematic. The parameters $\alpha_0^{\Sigma^+}$, $\alpha_+^{\Sigma^+}$, and α^{Σ^0} denote the decay asymmetry parameters for the processes $\Sigma^+ \rightarrow p\pi^0$, $\Sigma^+ \rightarrow n\pi^+$, and $\Sigma^0 \rightarrow \gamma\Lambda$, respectively. A_{CP}^{Σ} represents the CP observable, determined from the corresponding decay parameters.

Parameter	$J/\psi/\psi(3686) \rightarrow \Sigma^+\bar{\Sigma}^- \rightarrow p\pi^0\bar{p}\pi^0$ [50]	$J/\psi \rightarrow \Sigma^+\bar{\Sigma}^- \rightarrow n\pi^+(p\pi^0)\bar{p}\pi^0(\bar{n}\pi^-)$ [51]	$J/\psi/\psi(3686) \rightarrow \Sigma^0\bar{\Sigma}^0 \rightarrow \gamma\Lambda\gamma\bar{\Lambda}$ [54]
$\alpha_{J/\psi}$	$-0.5047 \pm 0.0018 \pm 0.0010$	$-0.5156 \pm 0.0030 \pm 0.0061$	$-0.4133 \pm 0.0035 \pm 0.0077$
$\Delta\Phi_{J/\psi}(\text{rad})$	$-0.2744 \pm 0.0033 \pm 0.0010$	$-0.2772 \pm 0.0044 \pm 0.0041$	$-0.0828 \pm 0.0068 \pm 0.0033$
$\alpha_{\psi(3686)}$	$0.7133 \pm 0.0094 \pm 0.0065$	—	$0.814 \pm 0.028 \pm 0.028$
$\Delta\Phi_{\psi(3686)}(\text{rad})$	$0.427 \pm 0.022 \pm 0.003$	—	$0.512 \pm 0.085 \pm 0.034$
$\alpha_0^{\Sigma^+}$	$-0.975 \pm 0.011 \pm 0.002$	—	—
$\alpha_0^{\Sigma^-}$	$0.999 \pm 0.011 \pm 0.004$	—	—
α^{Σ^0}	—	—	$-0.0017 \pm 0.0021 \pm 0.0018$
α^{Σ^0}	—	—	$0.0021 \pm 0.0020 \pm 0.0022$
$\alpha_+^{\Sigma^+}$	—	$0.0481 \pm 0.0031 \pm 0.0019$	—
$\alpha_-^{\Sigma^-}$	—	$-0.0565 \pm 0.0047 \pm 0.0022$	—
$\alpha_+^{\Sigma^+}/\alpha_0^{\Sigma^+}$	—	$-0.0490 \pm 0.0032 \pm 0.0021$	—
$\alpha_-^{\Sigma^-}/\alpha_0^{\Sigma^-}$	—	$-0.0571 \pm 0.0053 \pm 0.0032$	—
A_{CP}^{Σ}	$-0.0118 \pm 0.0083 \pm 0.0028$	$-0.080 \pm 0.052 \pm 0.028$	$0.0004 \pm 0.0029 \pm 0.0013$
α_-^{Λ}	—	—	$0.730 \pm 0.051 \pm 0.011$
α_+^{Λ}	—	—	$-0.776 \pm 0.054 \pm 0.010$
A_{CP}^{Λ}	—	—	$-0.030 \pm 0.069 \pm 0.015$

The additional weak decays of the Ξ^- and Ξ^0 hyperons allow the extraction of their weak phases ϕ_{Ξ^-} and ϕ_{Ξ^0} , as well as the strong and weak phase differences between the S -wave and P -wave amplitudes, thereby providing access to more CP observables [55–60]. The corresponding polarization signals are shown in Figure 2d,e, and the results are summarized in Table 2. Notably, the results for the J/ψ and $\psi(3686)$ decays to $\Xi^0\bar{\Xi}^0$ exhibit a significant difference, which may provide an important probe into the decay dynamics of charmonium decays to hyperon pairs. Similar to the case of Σ^+ , a polarization measurement for single-sided neutron decays has been performed based on the process $J/\psi \rightarrow \Xi^-\bar{\Xi}^+ \rightarrow \Lambda(p\pi^-)\pi^-\bar{\Lambda}(\bar{n}\pi^0)\pi^+$ and its charge-conjugate channel [61]. The decay parameters α_-^{Λ} (α_+^{Λ}) and α_0^{Λ} ($\alpha_0^{\bar{\Lambda}}$) of the two Λ decay modes are measured separately. Also, the ratios $\alpha_0^{\Lambda}/\alpha_-^{\Lambda}$ and $\alpha_0^{\bar{\Lambda}}/\alpha_+^{\Lambda}$, serving as observables for testing the $\Delta I = 1/2$ rule, are found to be smaller than the unity by more than 5σ . The corresponding CP observables A_{CP}^- and A_{CP}^0 are used to test CP symmetry. Furthermore, by taking the isospin-averaged value of the Λ decays, $A_{CP}^{\Lambda} = (2A_{CP}^- + A_{CP}^0)/3$, a more precise test of CP symmetry can be achieved. The relevant results are also summarized in Table 2.

The angular distribution analysis method can also be applied to high-spin hyperons. The discovery of the Ω^- was a major triumph for the eightfold way model of baryons, and angular distribution analysis provides a means to test the predictions of the eightfold way and the quark model regarding the spin of the Ω^- . Recently, the BESIII experiment performed a model-independent measurement of the Ω^- spin using the reaction $\psi(3686) \rightarrow \Omega^-\bar{\Omega}^+$ with the subsequent decays $\Omega^- \rightarrow K^-\Lambda$ and $\Lambda \rightarrow p\pi^-$ [62]. The Ω^- spin is determined to be $J = 3/2$, with a statistical significance of 14σ over the $J = 1/2$ hypothesis, as shown in Figure 3 (left). This represents the first establishment of the Ω^- spin that is independent of any model-based assumptions since its discovery more than fifty years ago. Additionally, the Ω^- particles exhibit not only vector polarization, but also quadrupole and octupole polarization contributions [39,63]. Accordingly, the helicity amplitudes and the $\cos\theta_{\Omega^-}$ dependence of the multipolar polarization operators were determined, as listed in Figure 3 (right) and Table 3. Note that, since a single-tag method is adopted for event reconstruction in this analysis, multiple solutions exist [64]. In addition, based on the decays $\Omega^- \rightarrow \Xi^0\pi^-$ and $\Omega^- \rightarrow \Xi^-\pi^0$, the $\Delta I = 1/2$ rule can also be tested through

the ratio of their branching fractions. A BESIII measurement reports $\mathcal{B}(\Omega^- \rightarrow \Xi^0 \pi^-) = (25.03 \pm 0.44 \pm 0.53)\%$, $\mathcal{B}(\Omega^- \rightarrow \Xi^- \pi^0) = (8.43 \pm 0.52 \pm 0.28)\%$, and $\mathcal{B}(\Omega^- \rightarrow \Lambda K^-) = (66.3 \pm 0.8 \pm 2.0)\%$ [65]. The ratio of $\mathcal{B}(\Omega^- \rightarrow \Xi^0 \pi^-)$ to $\mathcal{B}(\Omega^- \rightarrow \Xi^- \pi^0)$ is determined to be $2.97 \pm 0.19 \pm 0.11$, providing evidence for a deviation from the prediction of the $\Delta I = 1/2$ rule.

Table 2. Fitting results of each decay parameter for $J/\psi/\psi(3686) \rightarrow \Xi^-\bar{\Xi}^+$ and $J/\psi/\psi(3686) \rightarrow \Xi^0\bar{\Xi}^0$. The first uncertainty is statistical and the second is systematic. The superscript or subscript $\Xi(\bar{\Xi})$ denotes $\Xi^-(\bar{\Xi}^+)$ or $\Xi^0(\bar{\Xi}^0)$, corresponding to the respective decay mode. α_-^Λ (α_+^Λ) denotes the decay parameter of the dominant decay mode $\Lambda \rightarrow p\pi^-$ ($\bar{\Lambda} \rightarrow \bar{p}\pi^+$), while α_0^Λ ($\bar{\alpha}_0^\Lambda$) represents that of the $\Lambda \rightarrow n\pi^0$ ($\bar{\Lambda} \rightarrow \bar{n}\pi^0$) decay.

Parameter	$J/\psi \rightarrow \Xi^-\bar{\Xi}^+$ [57]	$J/\psi \rightarrow \Xi^-\bar{\Xi}^+ (\Lambda \rightarrow n\pi^0)$ [61]	$J/\psi \rightarrow \Xi^0\bar{\Xi}^0$ [55]	$\psi(3686) \rightarrow \Xi^-\bar{\Xi}^+$ [58]	$\psi(3686) \rightarrow \Xi^0\bar{\Xi}^0$ [56]
α_ψ	0.586 $\pm 0.012 \pm 0.010$	0.611 $\pm 0.007^{+0.013}_{-0.007}$	0.514 $\pm 0.006 \pm 0.015$	0.693 $\pm 0.048 \pm 0.049$	0.768 $\pm 0.029 \pm 0.025$
$\Delta\Phi$ (rad)	1.213 $\pm 0.046 \pm 0.016$	1.30 $\pm 0.03^{+0.02}_{-0.03}$	1.168 $\pm 0.019 \pm 0.018$	0.667 $\pm 0.111 \pm 0.058$	0.257 $\pm 0.061 \pm 0.009$
α_Ξ	$-0.376 \pm 0.007 \pm 0.003$	$-0.367 \pm 0.004^{+0.003}_{-0.004}$	$-0.3750 \pm 0.0034 \pm 0.0016$	$-0.344 \pm 0.025 \pm 0.007$	$-0.345 \pm 0.015 \pm 0.003$
$\alpha_{\bar{\Xi}}$	0.371 $\pm 0.007 \pm 0.002$	0.374 $\pm 0.004^{+0.003}_{-0.004}$	0.3790 $\pm 0.0034 \pm 0.0021$	0.355 $\pm 0.025 \pm 0.002$	0.355 $\pm 0.015 \pm 0.002$
ϕ_Ξ (rad)	0.011 $\pm 0.019 \pm 0.009$	$-0.016 \pm 0.012^{+0.004}_{-0.008}$	0.0051 $\pm 0.0096 \pm 0.0018$	0.023 $\pm 0.074 \pm 0.003$	0.008 $\pm 0.041 \pm 0.002$
$\phi_{\bar{\Xi}}$ (rad)	$-0.021 \pm 0.019 \pm 0.007$	0.010 $\pm 0.012^{+0.003}_{-0.013}$	$-0.0053 \pm 0.0097 \pm 0.0019$	$-0.123 \pm 0.073 \pm 0.004$	$-0.009 \pm 0.040 \pm 0.004$
α_-^Λ	0.757 $\pm 0.011 \pm 0.008$	0.764 $\pm 0.008^{+0.005}_{-0.006}$	0.7551 $\pm 0.0052 \pm 0.0023$	—	—
α_+^Λ	$-0.763 \pm 0.011 \pm 0.007$	$-0.774 \pm 0.009^{+0.005}_{-0.005}$	$-0.7448 \pm 0.0052 \pm 0.0017$	—	—
α_0^Λ	—	0.670 $\pm 0.009^{+0.009}_{-0.008}$	—	—	—
$\bar{\alpha}_0^\Lambda$	—	$-0.668 \pm 0.008^{+0.006}_{-0.008}$	—	—	—
$\alpha_0^\Lambda/\alpha_-^\Lambda$	—	0.877 $\pm 0.015^{+0.014}_{-0.010}$	—	—	—
$\alpha_0^\Lambda/\alpha_+^\Lambda$	—	0.863 $\pm 0.014^{+0.012}_{-0.008}$	—	—	—
$A_{CP}^\Xi (\times 10^{-2})$	0.60 $\pm 1.34 \pm 0.56$	$-0.9 \pm 0.8^{+0.7}_{-0.2}$	$-0.54 \pm 0.65 \pm 0.31$	$-1.5 \pm 5.1 \pm 1.0$	$-0.014 \pm 0.030 \pm 0.010$
$A_{CP}^{\bar{\Xi}} (\times 10^{-3})$	$-4 \pm 12 \pm 9$	$-7 \pm 8^{+2}_{-3}$	6.9 $\pm 5.8 \pm 1.8$	—	—
$A_{CP}^0 (\times 10^{-3})$	—	$1 \pm 9^{+5}_{-7}$	—	—	—
$A_{CP}^\Lambda (\times 10^{-3})$	—	$-4 \pm 7^{+3}_{-4}$	—	—	—
$\Delta\phi_{CP}^\Xi (\times 10^{-2} \text{ rad})$	$-0.48 \pm 1.37 \pm 0.29$	$-0.3 \pm 0.8^{+0.3}_{-0.7}$	$-0.1 \pm 6.9 \pm 0.9$	$-5.0 \pm 5.2 \pm 0.3$	$0.000 \pm 0.028 \pm 0.003$
$\delta_p - \delta_s (\times 10^{-1} \text{ rad})$	$-0.40 \pm 0.33 \pm 0.17$	$0.33 \pm 0.20^{+0.08}_{-0.12}$	$-0.13 \pm 0.17 \pm 0.4$	$-2.0 \pm 1.3 \pm 0.1$	$-0.022 \pm 0.078 \pm 0.011$
$\xi_p - \xi_s (\times 10^{-1} \text{ rad})$	$0.12 \pm 0.34 \pm 0.08$	$0.07 \pm 0.20^{+0.18}_{-0.05}$	0.00 $\pm 0.17 \pm 0.02$	—	$0.001 \pm 0.076 \pm 0.011$

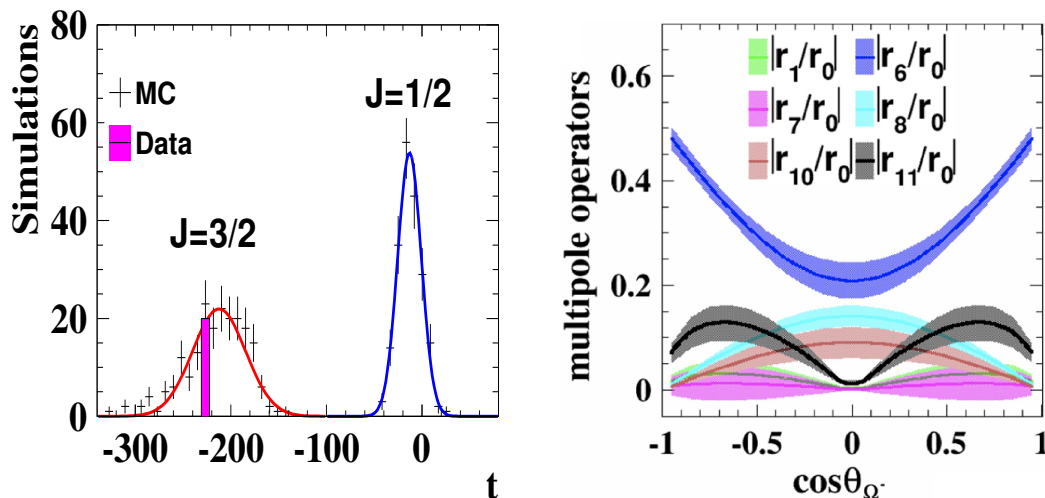


Figure 3. Distribution of the test statistic $t = S^{J=1/2} - S^{J=3/2}$ (left), where the curves denote Gaussian fits to the simulated samples and the vertical bar marks the value of t obtained from data. The dependence of the multipolar polarization operators on $\cos\theta_{\Omega^-}$ (right), where the solid lines represent the central values, and the shaded areas represent the range within one standard deviation [62].

Table 3. Summary of the fitted values of helicity parameters in $\psi(3686) \rightarrow \Omega^-\bar{\Omega}^+$ with the spin-3/2 hypothesis [62]. The first uncertainties are statistical, and the second ones are systematic.

Parameter	Solution I	Solution II
h_1	$0.30 \pm 0.11 \pm 0.04$	$0.31 \pm 0.10 \pm 0.04$
ϕ_1	$0.69 \pm 0.41 \pm 0.13$	$2.38 \pm 0.37 \pm 0.13$
h_3	$0.26 \pm 0.05 \pm 0.02$	$0.27 \pm 0.05 \pm 0.01$
ϕ_3	$2.60 \pm 0.16 \pm 0.08$	$2.57 \pm 0.16 \pm 0.04$
h_4	$0.51 \pm 0.03 \pm 0.01$	$0.51 \pm 0.03 \pm 0.01$
ϕ_4	$0.34 \pm 0.80 \pm 0.31$	$1.37 \pm 0.68 \pm 0.16$
ϕ_Ω	$4.29 \pm 0.45 \pm 0.23$	$4.15 \pm 0.44 \pm 0.16$

3.3. e^+e^- Annihilation

According to Equation (2), the angular distribution parameter is related to the moduli of the EMFFs. Using the measured angular distribution parameter (denoted as η for the non-resonant process), the modulus ratio R of the EMFFs can be directly calculated as [66]

$$R = \frac{|G_E|}{|G_M|} = \sqrt{\frac{\tau(1-\eta)}{1+\eta}}, \quad (8)$$

where $\tau = s/4M^2$, and M is the hyperon mass. Variations in the value of R correspond to different production mechanisms of hyperons. To investigate the production mechanisms and internal structure of hyperons under different interactions, BESIII performed angular distribution analyses of Λ and Σ^+ hyperon pairs at energies near the threshold, around the $\psi(3686)$ and $\psi(3770)$ resonances, covering both purely electromagnetic interactions and mixed electromagnetic-strong interactions.

For the Λ hyperon, a study of the purely electromagnetic process was performed at $\sqrt{s} = 2.396$ GeV [67], and the distribution of the polarization observable is shown in Figure 4a. Measurements near the $\psi(3686)$ [68] and $\psi(3770)$ [69,70] resonances are shown in Figure 4d–f. For the Σ^+ hyperon, studies are currently available only near the threshold [71] and around the $\psi(3686)$ [72] resonance. The corresponding polarization signals are shown in Figure 4b,c,g. All of the above measurement results are summarized in Table 4. These studies provide valuable insights into the production mechanisms of Λ and Σ^+ hyperon pairs at different c.m. energies.

Table 4. The measured parameters of $e^+e^- \rightarrow \Lambda\bar{\Lambda}$ [67,68,70] and $e^+e^- \rightarrow \Sigma^+\bar{\Sigma}^-$ [71,72] at each energy point. The first uncertainty is statistical and the second is systematic.

\sqrt{s} (GeV)	η	$\Delta\Phi$ (°)	R
$e^+e^- \rightarrow \Lambda\bar{\Lambda}$			
2.396	$0.12 \pm 0.14 \pm 0.02$	$37 \pm 12 \pm 6$	$0.96 \pm 0.14 \pm 0.02$
3.68–3.71	$0.69^{+0.07}_{-0.07} \pm 0.02$	$23^{+8.8}_{-8.0} \pm 1.6$	$0.71^{+0.10}_{-0.10} \pm 0.03$
3.773	$0.86 \pm 0.05 \pm 0.03$	$88 \pm 21 \pm 2$	$0.47 \pm 0.08 \pm 0.05$
$e^+e^- \rightarrow \Sigma^+\bar{\Sigma}^-$			
2.396	$-0.47 \pm 0.18 \pm 0.09$	$-42 \pm 22 \pm 14 \quad (-138 \pm 22 \pm 14)$	$1.69 \pm 0.38 \pm 0.20$
2.645	$0.41 \pm 0.12 \pm 0.06$	$55 \pm 19 \pm 14$	$0.72 \pm 0.11 \pm 0.06$
2.900	$0.35 \pm 0.17 \pm 0.15$	$78 \pm 22 \pm 9$	$0.85 \pm 0.16 \pm 0.15$
3.682	$0.54 \pm 0.17 \pm 0.12$	$22 \pm 23 \pm 7$	$0.84 \pm 0.20 \pm 0.14$
3.683	$0.96 \pm 0.13 \pm 0.12$	$135 \pm 95 \pm 7$	$0.22 \pm 0.37 \pm 0.34$
3.684	$0.86 \pm 0.15 \pm 0.12$	$68 \pm 35 \pm 7$	$0.42 \pm 0.21 \pm 0.20$
3.685	$0.76 \pm 0.10 \pm 0.12$	$9 \pm 18 \pm 7$	$0.57 \pm 0.15 \pm 0.16$
3.687	$0.66 \pm 0.12 \pm 0.12$	$1 \pm 15 \pm 7$	$0.70 \pm 0.15 \pm 0.15$
3.691	$0.16 \pm 0.23 \pm 0.12$	$74 \pm 31 \pm 7$	$1.31 \pm 0.30 \pm 0.16$
3.710	$0.01 \pm 0.40 \pm 0.12$	$-151 \pm 34 \pm 7$	$1.55 \pm 0.62 \pm 0.19$

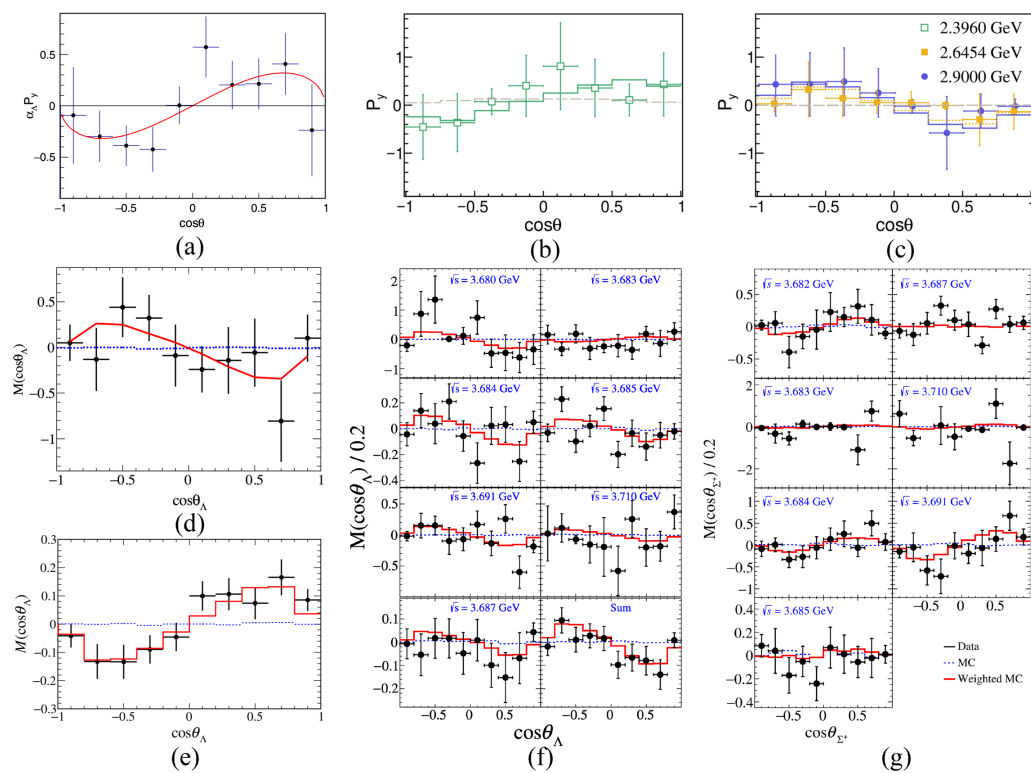


Figure 4. Distributions of the polarization observables P_y for $e^+e^- \rightarrow \Lambda\bar{\Lambda}$ at $\sqrt{s} = 2.396$ GeV [67] (a) and $e^+e^- \rightarrow \Sigma^+\bar{\Sigma}^-$ at $\sqrt{s} = 2.396\text{--}2.900$ GeV [71] (b,c), and M for $e^+e^- \rightarrow \Lambda\bar{\Lambda}$ at $\sqrt{s} = 3.773$ GeV [69,70] (d,e) and $3.68\text{--}3.71$ GeV [68] (f) and $e^+e^- \rightarrow \Sigma^+\bar{\Sigma}^-$ at $\sqrt{s} = 3.68\text{--}3.71$ GeV [72] (g), as functions of $\cos\theta$ for each process. The dots with error bars represent the experimental data, the red curve shows the global fit, the gray and blue dashed histograms correspond to the PHSP MC, and the red polyline and colored solid histograms show the PHSP MC weighted according to the global fit.

3.4. Electric Dipole Moment

Furthermore, if we introduce four form factors, F_V , H_σ , F_A , and H_T , representing the Dirac, Pauli, parity violation, and electric dipole form factors, respectively, the amplitude of the hyperon pair production process can be written as follows [73,74]:

$$\mathcal{A}^\mu = \bar{u}(p_1) [\gamma^\mu F_V + \frac{i}{2M} \sigma^{\mu\nu} q_\nu H_\sigma + \gamma^\mu \gamma^5 F_A + \sigma^{\mu\nu} q_\nu \gamma^5 H_T] v(p_2), \quad (9)$$

where p_1 , p_2 , and M follow the same definitions as in Equation (1). Parity conservation implies $F_A = 0$, while CP conservation further implies $H_T = 0$. The form factors F_V and H_σ are related to the EMFFs with $F_V = G_M - 4M^2 \frac{G_M - G_E}{(p_1 - p_2)^2}$ and $H_\sigma = 4M^2 \frac{G_M - G_E}{(p_1 - p_2)^2}$, while H_T can be associated with the hyperon electric dipole moment (EDM) [73,74]. Based on this approach, a joint angular distribution can be constructed to explore CP violation in a novel way, while simultaneously determining the hyperon EDM. Recently, BESIII performed an analysis based on the $J/\psi \rightarrow \Lambda\bar{\Lambda}$ process, using F_A and H_T as observables to explore both P and CP violation, while also making a precise measurement of the EDM of Λ [75]. The corresponding results are shown in Table 5. This measurement improves the sensitivity to the Λ EDM by three orders of magnitude compared to previous results, while also introducing a new approach to probing possible sources of CP violation.

Table 5. Summary of fitted parameters [75]. The first uncertainty is statistical and the second is systematic.

Parameter	Fitting Results
P_L	$(-1.8 \pm 1.2 \pm 0.8) \times 10^{-3}$
$Re(F_A)$	$(-2.4 \pm 1.6 \pm 3.1) \times 10^{-6}$
$Im(F_A)$	$(-7.9 \pm 3.7 \pm 2.5) \times 10^{-6}$
$Re(H_T)$ (GeV $^{-1}$)	$(-1.4 \pm 1.4 \pm 0.2) \times 10^{-6}$
$Im(H_T)$ (GeV $^{-1}$)	$(1.3 \pm 1.2 \pm 0.4) \times 10^{-6}$
$Re(d_\Lambda)$ (cm)	$(-3.1 \pm 3.2 \pm 0.5) \times 10^{-19} e$
$Im(d_\Lambda)$ (cm)	$(2.9 \pm 2.6 \pm 0.6) \times 10^{-19} e$

4. Hyperon Rare Decay

4.1. Radiative Decay

The radiative decays of hyperons offer important insights into the properties of non-leptonic weak interactions [76]. In the limit of unitary symmetry, the parity-violating amplitude in these decays is expected to be small, resulting in a decay asymmetry parameter of $\alpha_\gamma = 0$ [77]. However, experimental measurements show that the values of α_γ are large. Several phenomenological models have been proposed to account for these results [78–84]; nevertheless, none has yet provided a unified description of all weak radiative hyperon decays. To enrich the available experimental information, BESIII has also carried out a series of studies on radiative hyperon decays.

Based on the processes $J/\psi \rightarrow \Lambda\bar{\Lambda}$, $\Sigma^+\bar{\Sigma}^-$, and $\Xi^0\bar{\Xi}^0$, the branching fractions and decay asymmetry parameters of the decays $\Lambda \rightarrow n\gamma$, $\Sigma^+ \rightarrow p\gamma$, and $\Xi^0 \rightarrow \Lambda\gamma$ were measured [85–87]. Compared with previous results, the precision of these measurements has been significantly improved, and the decay asymmetry parameter of $\Lambda \rightarrow n\gamma$ has been determined for the first time. The measured results are summarized in Table 6. These measurements serve as valuable tests of various phenomenological models. A comparison between the BESIII results, the PDG averages, and the model predictions is presented in Figure 5. In addition, CP tests were performed in these analyses by constructing observables from the α_γ values of hyperons and antihyperons. Within the current statistical precision, the results are consistent with CP symmetry.

Table 6. Results of branching fractions and α_γ for each radiative decay obtained from both individual and simultaneous fits [85–87]. The first uncertainties are statistical and the second uncertainties are systematic.

Mode	$\Lambda \rightarrow n\gamma$	$\bar{\Lambda} \rightarrow \bar{n}\gamma$
Individual BF (10 $^{-3}$)	$0.820 \pm 0.045 \pm 0.066$	$0.862 \pm 0.071 \pm 0.084$
Simultaneous BF (10 $^{-3}$)	$0.832 \pm 0.038 \pm 0.054$	
Individual α_γ	$-0.13 \pm 0.13 \pm 0.03$	$0.21 \pm 0.15 \pm 0.06$
Simultaneous α_γ	$-0.16 \pm 0.010 \pm 0.05$	
Mode	$\Sigma^+ \rightarrow p\gamma$	$\bar{\Sigma}^- \rightarrow \bar{p}\gamma$
Individual BF (10 $^{-3}$)	1.005 ± 0.032	0.993 ± 0.030
Simultaneous BF (10 $^{-3}$)	$0.996 \pm 0.021 \pm 0.018$	
Individual α_γ	-0.587 ± 0.082	0.710 ± 0.076
Simultaneous α_γ	$-0.651 \pm 0.056 \pm 0.020$	
Mode	$\Xi^0 \rightarrow \Lambda\gamma$	$\bar{\Xi}^0 \rightarrow \bar{\Lambda}\gamma$
Individual BF (10 $^{-3}$)	$1.348 \pm 0.090 \pm 0.054$	$1.326 \pm 0.098 \pm 0.066$
Simultaneous BF (10 $^{-3}$)	$1.347 \pm 0.066 \pm 0.054$	
Individual α_γ	$-0.652 \pm 0.092 \pm 0.016$	$0.830 \pm 0.080 \pm 0.044$
Simultaneous α_γ	$-0.741 \pm 0.062 \pm 0.019$	

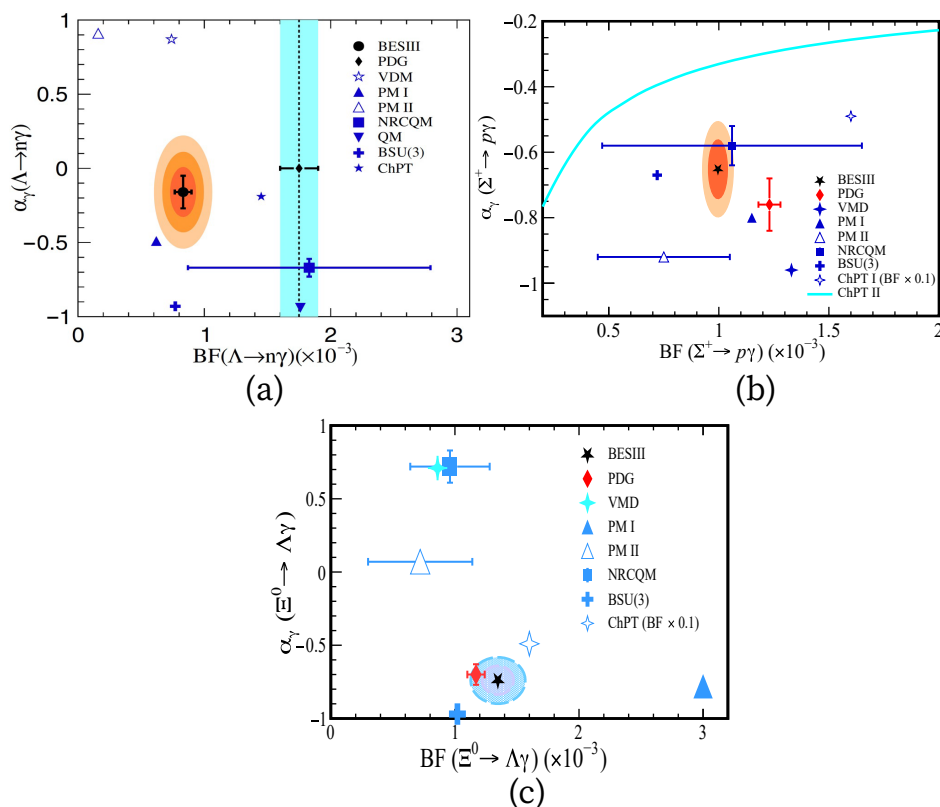


Figure 5. Distributions of α_γ versus branching fraction for $\Lambda \rightarrow n\gamma$ [85] (a), $\Sigma^+ p\gamma$ [86] (b), and $\Xi^0 \rightarrow \Lambda\gamma$ [87] (c), along with the PDG values [88] and predictions from the vector meson dominance model (VDM) [80], pole model (PM I [78] and PM II [79]), nonrelativistic constituent quark model (NRCQM) [83], broken SU(3) model [BSU(3)] [82], and chiral perturbation theory (ChPT) [81,84].

4.2. Semileptonic Decay

The general approach to determining the absolute branching fractions of rare hyperon decays is to extract the signal yields and detection efficiencies using both the single-tag (ST) and double-tag (DT) methods, and then to obtain the branching fraction as

$$\mathcal{B}_{sig} = \frac{N_{DT}/\epsilon_{DT}}{N_{ST}/\epsilon_{ST}}, \quad (10)$$

where N_{ST} (N_{DT}) denotes the ST (DT) yield, and ϵ_{ST} (ϵ_{DT}) denotes the corresponding ST (DT) detection efficiency. Based on this method, a study using the process $J/\psi \rightarrow \Xi^0 \bar{\Xi}^0$ was carried out at BESIII to search for the baryon and lepton number violating decays $\Xi^0 \rightarrow K^- e^+$ and $\Xi^0 \rightarrow K^+ e^-$ [89]. Since no evidence for either decay was observed in this analysis, upper limits on their branching fractions at the 90% confidence level (C.L.) were reported to be $\mathcal{B}(\Xi^0 \rightarrow K^- e^+) < 3.6 \times 10^{-6}$ and $\mathcal{B}(\Xi^0 \rightarrow K^+ e^-) < 1.9 \times 10^{-6}$.

BESIII has also investigated the semileptonic decays of the Λ [90], Ξ^- [91], and Ξ^0 [92] hyperons. The decays $\Lambda \rightarrow p\mu^- \bar{\nu}_\mu$ and $\Lambda \rightarrow p e^- \bar{\nu}_e$ provide an excellent opportunity to test lepton flavor universality (LFU) and thereby to examine the validity of the SM [93]. The ratio of the decay rates of these two processes $R^{\mu e} \equiv [\Gamma(\Lambda \rightarrow p\mu^- \bar{\nu}_\mu)] / [\Gamma(\Lambda \rightarrow p e^- \bar{\nu}_e)]$ serves as an observable for testing LFU. However, previous results are still based on fixed-target experiments and therefore suffer from relatively large uncertainties. Using a data sample of 10 billion J/ψ events and the decay $J/\psi \rightarrow \Lambda \bar{\Lambda}$, BESIII has measured the absolute branching fraction of $\Lambda \rightarrow p\mu^- \bar{\nu}_\mu$ to be $\mathcal{B}(\Lambda \rightarrow p\mu^- \bar{\nu}_\mu) = (1.48 \pm 0.21 \pm 0.08) \times 10^{-4}$, achieving a 30% improvement in precision compared to the world average. Based on the well-measured branching fraction of $\Lambda \rightarrow p e^- \bar{\nu}_e$, the ratio $R^{\mu e}$ is determined to be 0.178 ± 0.028 , which is consistent with previous results and with LFU [88,94]. Meanwhile,

a CP test is also performed using the asymmetry $A_{CP} = \frac{\mathcal{B}(\Lambda \rightarrow p\mu^-\bar{\nu}_\mu) - \mathcal{B}(\bar{\Lambda} \rightarrow \bar{p}\mu^+\nu_\mu)}{\mathcal{B}(\Lambda \rightarrow p\mu^-\bar{\nu}_\mu) + \mathcal{B}(\bar{\Lambda} \rightarrow \bar{p}\mu^+\nu_\mu)}$, which is determined to be $A_{CP} = 0.02 \pm 0.14 \pm 0.02$, consistent with CP conservation. In addition, using the same J/ψ decay sample, the processes $\Xi^- \rightarrow \Xi^0 e^- \bar{\nu}_e$ and $\Xi^0 \rightarrow \Sigma^- e^+ \nu_e$ have also been investigated at BESIII. Since no significant signal is observed, upper limits on their branching fractions at 90% C.L. are reported, given by $\mathcal{B}(\Xi^- \rightarrow \Xi^0 e^- \bar{\nu}_e) < 2.59 \times 10^{-4}$ and $\mathcal{B}(\Xi^0 \rightarrow \Sigma^- e^+ \nu_e) < 1.6 \times 10^{-4}$. These results also provide important experimental constraints for the study of the SU(3) symmetry-breaking mechanism, $\Delta S = \Delta Q$ -violating decays, and other rare or forbidden hyperon decays.

5. Hyperon Pair Production

In recent years, measurements of cross sections near production thresholds have provided a sensitive probe for exploring particle interactions, electromagnetic form factors, and possible new resonance states. Numerous experimental studies have been carried out to explore baryon properties, with most analyses based on the interpretation of the Born cross section for baryon–antibaryon pair production. Notably, several of these measurements observed an unusual behavior near the threshold—a significantly nonzero cross section, commonly referred to as threshold enhancement. At BESIII, threshold enhancement has been observed in the measurements of the processes $e^+e^- \rightarrow p\bar{p}$ [95–97], $e^+e^- \rightarrow n\bar{n}$ [98], $e^+e^- \rightarrow \Lambda\bar{\Lambda}$ [99], and $e^+e^- \rightarrow \Lambda\bar{\Sigma}^0$ [100]. Similar threshold behavior has also been observed in the cross sections of $e^+e^- \rightarrow \Sigma\bar{\Sigma}$ [101,102] and $e^+e^- \rightarrow \Xi\bar{\Xi}$ [103,104], although larger data samples are required to draw more definitive conclusions. In addition, measurements of $e^+e^- \rightarrow \Omega^-\bar{\Omega}^+$ have also been performed [105]. However, since the available energy points are relatively far from the production threshold, no evident threshold enhancement has been observed in this case. In these studies, the Born cross sections and effective form factors of each process were measured using either energy-scan or ISR methods, as shown in Figure 6 (left). In the measurements of the reactions of $e^+e^- \rightarrow p\bar{p}$ and $n\bar{n}$, oscillatory behavior of the effective form factors has also been observed, suggesting the presence of intrinsic dynamics that are not yet fully understood.

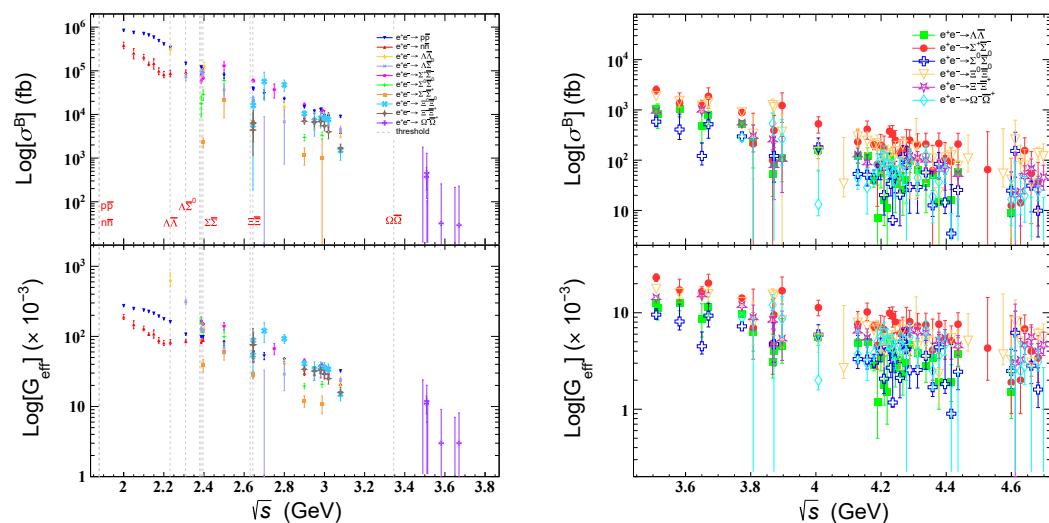


Figure 6. The Born cross sections and effective form factors for each baryon pair process near the threshold (left) and in the charmonium energy region (right). The gray dashed lines represent the production threshold of corresponding baryon pairs.

In the charmonium energy region, studying the hadronic decays of charmonium-like states by measuring the Born cross sections of baryonic final states is one of the key approaches to revealing their physical properties. The BESIII experiment performed its first search for the charmonium(-like) states $Y(4230/4260)$ in the process $e^+e^- \rightarrow \Xi^-\bar{\Xi}^+$

at c.m. energies ranging from 3.5 to 4.6 GeV [106], but found no significant evidence for $\Upsilon(4230/4260)$ decaying into $\Xi^-\bar{\Xi}^+$. Subsequently, BESIII has conducted a series of studies on hyperon pair production in the processes $e^+e^- \rightarrow \Lambda\bar{\Lambda}$, $\Sigma^+\bar{\Sigma}^-$, $\Sigma^0\bar{\Sigma}^0$, $\Xi^0\bar{\Xi}^0$, and $\Omega^-\bar{\Omega}^+$, along with an updated measurement of $\Xi^-\bar{\Xi}^+$ [107–113]. The Born cross sections and effective form factors for these processes were measured, as shown in Figure 6 (right). To further investigate the charmonium(-like) states, fits to the dressed cross sections were carried out. Evidence for the decays $\psi(3770) \rightarrow \Lambda\bar{\Lambda}$ and $\psi(3770) \rightarrow \Xi^-\bar{\Xi}^+$ was found [107,113], as shown in Figure 7a,b. The branching fractions of these two decays are determined to be $\mathcal{B}(\psi(3770) \rightarrow \Lambda\bar{\Lambda}) = (2.4^{+15.0}_{-1.9}) \times 10^{-5}$ or $(14.4^{+2.7}_{-14.0}) \times 10^{-5}$ and $\mathcal{B}(\psi(3770) \rightarrow \Xi^-\bar{\Xi}^+) = (136.0 \pm 35.2) \times 10^{-6}$, respectively. For the other processes, no significant signal of charmonium(-like) states was observed. Only upper limits for the product of the branching fraction and the electronic partial width, $\Gamma_{ee}\mathcal{B}$, at the 90% C.L., were evaluated. These measurements provide evidence for charmless decays of $\psi(3770)$ and can be useful for understanding the coupling of charmonium(-like) states to hyperon pair final states.

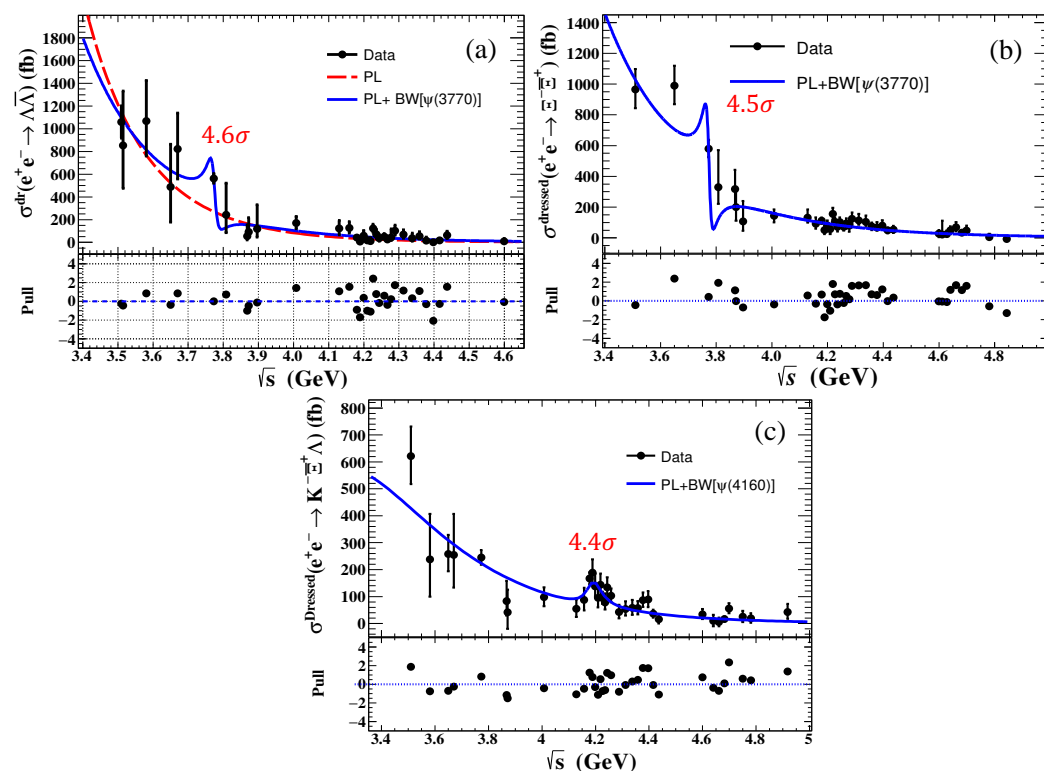


Figure 7. Fits to the dressed cross sections for the $e^+e^- \rightarrow \Lambda\bar{\Lambda}$ [107] (a), $\Xi^-\bar{\Xi}^+$ [113] (b), and $K^-\bar{\Xi}^+\Lambda$ [114] (c) reactions.

The BESIII experiment has also measured the Born cross sections for three-body decays with hyperon final states [114–118], as shown in Figure 8 (left). For these processes, no significant charmonium(-like) states were observed, except for evidence of the decay $\psi(4160) \rightarrow K^-\bar{\Xi}\Lambda + \text{c.c.}$, which was observed with a significance of 4.4σ , including systematic uncertainties, as shown in Figure 7c. The branching fraction $\mathcal{B}(\psi(4160) \rightarrow K^-\bar{\Xi}\Lambda + \text{c.c.})$ is determined to be $(4.4 \pm 2.1) \times 10^{-6}$. Similarly, upper limits on $\Gamma_{ee}\mathcal{B}$ are provided for other assumed resonances. In the processes $e^+e^- \rightarrow p\Lambda$, $\phi\Lambda\bar{\Lambda}$, and $\eta\Lambda\bar{\Lambda}$, clear enhancements can be seen in the invariant mass distributions of $p\Lambda$ and $\Lambda\bar{\Lambda}$ [115,117,118]. Based on fits with Breit–Wigner (BW) functions, the masses and widths of these near-threshold structures were determined, but they do not match any previously known resonances. Future studies

with larger data samples and theoretical analyses involving partial wave analysis may help clarify the nature of these observed structures.

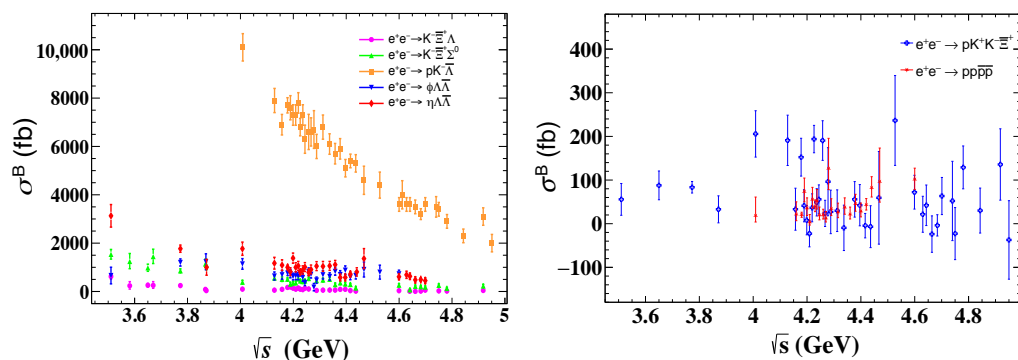


Figure 8. Line shapes of the measured Born cross sections for each three-body (left) and four-body (right) process.

In addition, some studies have focused on the multi-body processes $e^+e^- \rightarrow 2(p\bar{p})$ [119], $e^+e^- \rightarrow pp\bar{p}\bar{n}\pi^- + \text{c.c.}$ [120,121], and $e^+e^- \rightarrow pK^-K^+\bar{\Xi}^+$ [122], aiming to search for possible deuteron, hexaquark, or di-baryon candidates, as well as to explore charmonium(-like) states. Among these, the measurement results of the Born cross sections for the four-body processes are shown in Figure 8 (right). However, with the current statistics, no definitive conclusions can be drawn regarding the existence of actual resonances or structures in these analyses.

6. Hyperon Nucleon Interaction

Depending on the charmonium decay modes producing hyperons, and using neutrons in the beam-pipe material as targets, BESIII has pioneered a series of hyperon–nucleon scattering studies. The beam pipe, composed of gold (^{197}Au), beryllium (^9Be), and oil ($^{12}\text{C} : ^1\text{H} = 1 : 2.13$), provides a natural and effective target for such studies [123,124]. The hyperon–nucleon scattering process in an electron–positron collider is illustrated in Figure 9 [124]. Hyperon pairs or final states containing hyperons are produced inside the beam pipe and travel along their momentum direction. Some of these hyperons reach the target before decaying and undergo elastic or inelastic scattering with the nuclei in the material. However, due to the complexity of the materials in the beam pipe and the inner wall of the MDC, the BESIII experiment cannot directly extract hyperon–nucleon scattering cross sections as in fixed-target experiments. Therefore, ^9Be , which is commonly used in fixed-target experiments and is also the primary material of the beam pipe, is chosen as the normalization reference, and the cross sections of all materials are normalized to that on ^9Be .

The first study in this series observed the inelastic scattering process $\Xi^0 n \rightarrow \Xi^- p$ with a significance of 7.1σ , based on Ξ^0 hyperons produced in the decay $J/\psi \rightarrow \Xi^0\bar{\Xi}^0$ [125]. The reaction cross section of Ξ^0 with the ^9Be target in the beam pipe was measured at a Ξ^0 momentum of $0.818 \text{ GeV}/c$. Assuming an effective number of three reaction neutrons in a ^9Be nucleus, the cross section for the $\Xi^0 n \rightarrow \Xi^- p$ process was determined. The inelastic scattering process $\Lambda + ^9\text{Be} \rightarrow \Sigma^+ + X$ was also investigated [126]. The cross section was measured within the Λ momentum range of $[1.057, 1.091] \text{ GeV}/c$. The $\Lambda + p \rightarrow \Sigma^+ + X$ cross section was further determined under the assumption that the signal originates from a surface reaction. The result is consistent with previous experimental measurements. For the Λ hyperon, an elastic scattering study was also performed for the processes $\Lambda + p \rightarrow \Lambda + p$ and $\bar{\Lambda} + p \rightarrow \bar{\Lambda} + p$, representing the first investigation of anti-hyperon–nucleon scattering [127]. Within the angular region $-0.9 \leq \cos\theta_{\Lambda/\bar{\Lambda}} \leq 0.9$ and at

a $\Lambda/\bar{\Lambda}$ momentum of $1.074 \pm 0.017 \text{ GeV}/c$, the cross sections for these two processes were measured. Here, $\theta_{\Lambda/\bar{\Lambda}}$ denotes the scattering angle. However, the angular distributions of the cross sections for these two reactions exhibit distinctly different trends, as shown in Figure 10a,b. Theoretical studies attribute the observed difference to reaction dynamics [128]: the Λp process involves contributions from both the t and u channels, while the $\bar{\Lambda} p$ process allows only the t -channel, leading to the distinct trends observed. Here, the theoretical predictions are in good agreement with the experimental data, as shown in Figure 10c,d. A recent study has measured the inelastic scattering processes $\Sigma^+ n \rightarrow \Lambda p$ and $\Sigma^+ n \rightarrow \Sigma^0 p$ [129]. At a Σ^+ momentum of $0.992 \pm 0.015 \text{ GeV}/c$, the reaction cross sections with the ${}^9\text{Be}$ nucleus were measured, and assuming an effective number of three reaction neutrons, the single-neutron cross sections were determined to be in good agreement with theoretical predictions. The aforementioned measurements of the scattering cross section are summarized in Table 7.

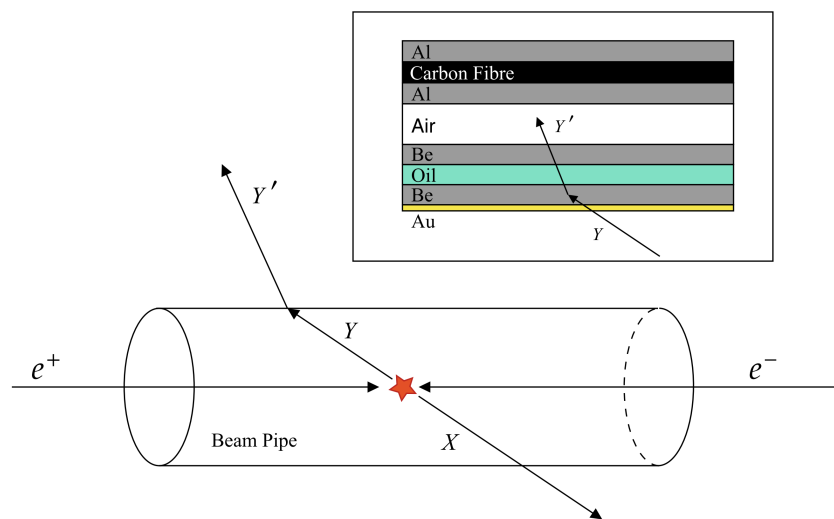


Figure 9. Schematic of the hyperon–nucleus interactions at the e^+e^- collider represented by BE-SIII [124]. Y and Y' denote the hyperon before and after scattering, respectively, while X represents the accompanying particles produced together with Y .

Table 7. The measured cross sections of hyperon–nucleon scattering [125–127,129]. The first uncertainty is statistical and the second is systematic.

Reaction	σ (mb)
$\Xi^0 + {}^9\text{Be} \rightarrow \Xi^- + p + {}^8\text{Be}$	$22.1 \pm 5.3 \pm 4.5$
$\Xi^0 + n \rightarrow \Xi^- + p$	$7.4 \pm 1.8 \pm 1.5$
$\Lambda + {}^9\text{Be} \rightarrow \Sigma^+ + X$	$37.3 \pm 4.7 \pm 3.5$
$\Lambda + p \rightarrow \Sigma^+ + X$	$19.3 \pm 2.4 \pm 1.8$
$\Lambda + p \rightarrow \Lambda + p$	$12.2 \pm 1.6 \pm 1.1$
$\bar{\Lambda} + p \rightarrow \bar{\Lambda} + p$	$17.5 \pm 2.1 \pm 1.6$
$\Sigma^+ + {}^9\text{Be} \rightarrow \Lambda + p + {}^8\text{Be}$	$45.2 \pm 12.1 \pm 7.2$
$\Sigma^+ + n \rightarrow \Lambda + p$	$15.1 \pm 4.0 \pm 2.4$
$\Sigma^+ + {}^9\text{Be} \rightarrow \Sigma^0 + p + {}^8\text{Be}$	$29.8 \pm 9.7 \pm 6.9$
$\Sigma^+ + n \rightarrow \Sigma^0 + p$	$9.9 \pm 3.2 \pm 2.3$

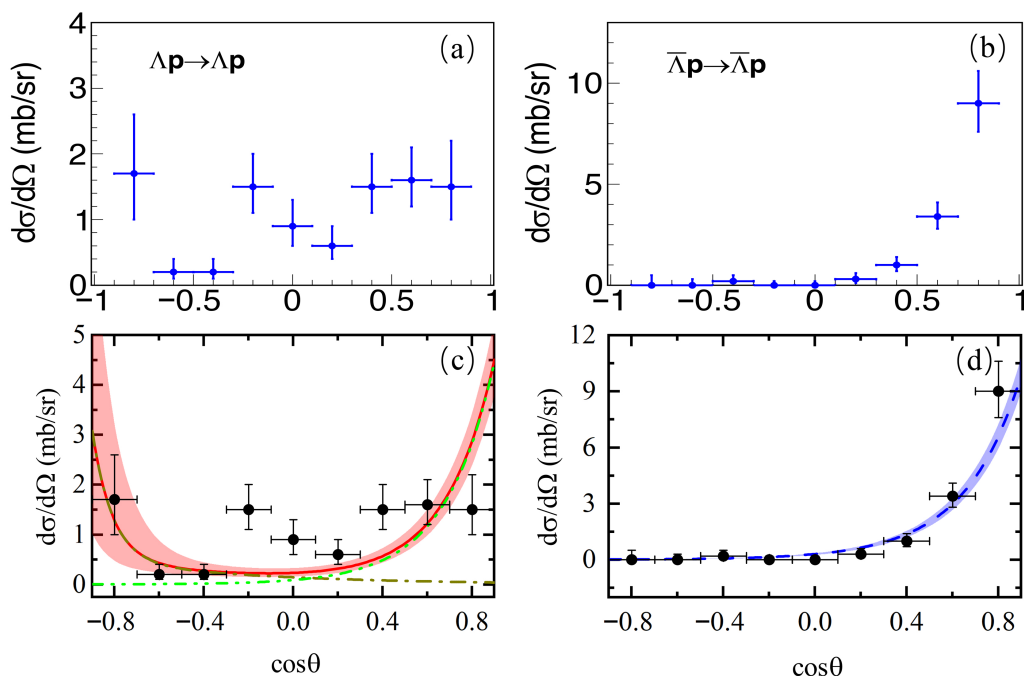


Figure 10. Differential cross sections for the reactions $\Lambda + p \rightarrow \Lambda + p$ (a,c) and $\bar{\Lambda} + p \rightarrow \bar{\Lambda} + p$ (b,d) [127,128]. The dots with error bars represent the experimental data. The solid red curve denotes the complete theoretical model, while the green dash-double-dotted and dark-yellow dash-dotted curves show the individual contributions from the t and u channels, respectively. The t -channel contribution is also displayed by the blue dashed curve.

7. Conclusions and Outlook

Having been operating successfully since 2008, the BESIII experiment has collected the world's largest data samples in the τ -charm physics region and has conducted a comprehensive program in hyperon physics. In studies of hyperon polarization, the angular distribution analysis method has been widely applied. Numerous polarization signals have been observed, CP violation observables have reached the 10^{-3} level, studies of form factors and radiative decays have provided insights into the interaction mechanisms, and the measurement of the Λ EDM has achieved unprecedented precision. In the field of rare hyperon decay studies, baryon and lepton number violating decays as well as semileptonic decays have been extensively investigated, providing stringent experimental constraints and precision tests of the SM. Extensive cross section measurements have been performed from the hyperon pair production threshold up to the charmonium energy region, including determinations of the relevant form factors for hyperon pair processes. Evidence for the decays $\psi(3770) \rightarrow \Lambda\bar{\Lambda}/\Xi^-\bar{\Xi}^+$ and $\psi(4160) \rightarrow K^-\bar{\Xi}^+\Lambda$ has also been reported. Moreover, an innovative experimental approach has been developed at BESIII to study hyperon–nucleon interactions, which has already been applied to various elastic and inelastic scattering processes. These studies have greatly enriched our understanding of the internal structure and interactions of hyperons. Looking ahead, the BESIII Collaboration is updating its hardware and continuing data collection, with several ongoing exciting analyses; more fascinating results are expected in the near future.

Author Contributions: Conceptualization and methodology, R.Z. and X.W. All authors have read and agreed to the published version of the manuscript.

Funding: This work was supported by the Fundamental Research Funds for the Central Universities Nos. lzujbky-2025-it06, lzujbky-2025-ytA05, lzujbky-2024-jdzx06; the Natural Science Foundation of

Gansu Province No. 22JR5RA389, No. 25JRRA799; the ‘111 Center’ under Grant No. B20063; and the National Natural Science Foundation of China under Contract No. 12247101.

Data Availability Statement: No new data were created or analyzed in this study. Data sharing is not applicable to this article.

Conflicts of Interest: The authors declare no conflicts of interest.

Abbreviations

The following abbreviations are used in this manuscript:

CP	Charge-conjugation and parity
CKM	Cabibbo–Kobayashi–Maskawa
BNV	Baryon-number-violating
EoS	Equation of state
c.m.	Center-of-mass
MDC	Multilayer drift chamber
TOF	Time-of-flight system
EMC	Electromagnetic calorimeter
c.c.	Charge-conjugation
PHSP	Phase space
MC	Monte Carlo
VMD	Vector meson dominance model
PM	Pole model
NRCQM	Nonrelativistic constituent quark model
BSU(3)	Broken SU(3) model
ChPT	Chiral perturbation theory
EDM	Electric dipole moment
C.L.	Confidence level
DT	Double-tag
ST	Single-tag
LFU	Lepton flavor universality

References

1. Dine, M.; Kusenko, A. Origin of the matter–antimatter asymmetry. *Rev. Mod. Phys.* **2003**, *76*, 1–30. [[CrossRef](#)]
2. Sakharov, A.D. Violation of CP invariance, C asymmetry, and baryon asymmetry of the universe. *Sov. Phys. Usp.* **1967**, *34*, 392–393. [[CrossRef](#)]
3. Christenson, J.H.; Cronin, J.W.; Fitch, V.L.; Turlay, R. Evidence for the 2π decay of the K_2^0 meson. *Phys. Rev. Lett.* **1964**, *13*, 138–140. [[CrossRef](#)]
4. Aubert, B.; Boutigny, D.; Gaillard, J.M.; Hicheur, A.; Karyotakis, Y.; Lees, J.P.; Robbe, P.; Tisserand, V.; Palano, A.; Chen, G.P.; et al. Observation of CP violation in the B^0 meson system. *Phys. Rev. Lett.* **2001**, *87*, 091801. [[CrossRef](#)] [[PubMed](#)]
5. Abe, K.; Abe, R.; Adachi, I.; Ahn, B.S.; Aihara, H.; Akatsu, M.; Alimonti, G.; Asai, K.; Asai, M.; Asano, Y.; et al. Observation of large CP violation in the neutral B meson system. *Phys. Rev. Lett.* **2001**, *87*, 091802. [[CrossRef](#)] [[PubMed](#)]
6. Aaij, R.; Beteta, C.A.; Adeva, B.; Adinolfi, M.; Aidala, C.A.; Ajaltouni, Z.; Akar, S.; Albicocco, P.; Albrecht, J.; Alessio, F.; et al. Observation of CP violation in charm decays. *Phys. Rev. Lett.* **2019**, *122*, 211803. [[CrossRef](#)]
7. Abe, K.; Akutsu, R.; Ali, A.; Alt, C.; Andreopoulos, C.; Anthony, L.; Antonova, M.; Aoki, S.; Ariga, A.; Arikara, T.; et al. Constraint on the matter–antimatter symmetry-violating phase in neutrino oscillations. *Nature* **2020**, *580*, 339–344. [[CrossRef](#)] [[PubMed](#)]
8. Cabibbo, N. Unitary Symmetry and Leptonic Decays. *Phys. Rev. Lett.* **1963**, *10*, 531–533. [[CrossRef](#)]
9. Kobayashi, M.; Maskawa, T. CP Violation in the Renormalizable Theory of Weak Interaction. *Prog. Theor. Phys.* **1973**, *49*, 652–657. [[CrossRef](#)]
10. Aaij, R.; Beteta, C.A.; Adeva, B.; Adinolfi, M.; Aidala, C.A.; Ajaltouni, Z.; Akar, S.; Albicocco, P.; Albrecht, J.; Alessio, F.; et al. Observation of charge–parity symmetry breaking in baryon decays. *Nature* **2025**, *643*, 1223–1228. [[CrossRef](#)]
11. Wang, X. Study of hyperon physics at BESIII. *Moscow Univ. Phys. Bull.* **2024**, *79*, 105–110. [[CrossRef](#)]
12. Punjabi, V.; Perdrisat, C.F.; Jones, M.K.; Brash, E.J.; Carlson, C.E. The Structure of the Nucleon: Elastic Electromagnetic Form Factors. *Eur. Phys. J. A* **2015**, *51*, 79. [[CrossRef](#)]

13. Brambilla, N.; Eidelman, S.; Hanhart, C.; Nefediev, A.; Shen, C.P.; Thomas, C.E.; Vairo, A.; Yuan, C.Z. The XYZ States: Experimental and Theoretical Status and Perspectives. *Phys. Rep.* **2020**, *873*, 1–154. [\[CrossRef\]](#)

14. Wang, X.; Liu, X.; Gao, Y. Colloquium: Hadron Production in Open-charm Meson Pair at e^+e^- Collider. *arXiv* **2025**, arXiv:2502.15117.

15. Brambilla, N.; Eidelman, S.; Heltsley, B.; Vogt, R.; Bodwin, G.T.; Eichten, E.; Frawley, A.D.; Meyer, A.B.; Mitchell, R.E.; Papadimitriou, V.; et al. Heavy Quarkonium: Progress, Puzzles, and Opportunities. *Eur. Phys. J. C* **2011**, *71*, 1534. [\[CrossRef\]](#)

16. Briceño, R.A.; Cohen, T.D.; Coito, S.; Dudek, J.J.; Eichten, E.; Fischer, C.S.; Fritsch, M.; Gradl, W.; Jackura, A.; Kornicer, M.; et al. Issues and Opportunities in Exotic Hadrons. *Chin. Phys. C* **2016**, *40*, 042001. [\[CrossRef\]](#)

17. Close, F.E.; Page, P.R. Gluonic charmonium resonances at BaBar and Belle. *Phys. Lett. B* **2005**, *628*, 215–222. [\[CrossRef\]](#)

18. Chen, H.X.; Chen, W.; Liu, X.; Zhu, S.L. The hidden-charm pentaquark and tetraquark states. *Phys. Rep.* **2016**, *639*, 1–121. [\[CrossRef\]](#)

19. Wang, J.Z.; Chen, D.Y.; Liu, X.; Matsuki, T. Constructing J/ψ family with updated data of charmoniumlike Y states. *Phys. Rev. D* **2019**, *99*, 114003. [\[CrossRef\]](#)

20. Qian, R.Q.; Huang, Q.; Liu, X. Predicted $\Lambda\bar{\Lambda}$ and $\Xi^-\bar{\Xi}^+$ decay modes of the charmoniumlike $Y(4230)$. *Phys. Lett. B* **2022**, *833*, 137292. [\[CrossRef\]](#)

21. Ablikim, M.; Achasov, M.N.; Ai, X.C.; Albayrak, O.; Albrecht, M.; Ambrose, D.J.; Amoroso, A.; An, F.F.; An, Q.; Bai, J.Z.; et al. Precise Measurement of Born Cross Sections for $e + e^- \rightarrow D\bar{D}$ at $\sqrt{s}=3.80\text{--}4.95$ GeV. *Phys. Rev. Lett.* **2024**, *133*, 081901. [\[CrossRef\]](#)

22. Wang, X. Recent Advances in Hadron Production in e^+e^- Annihilation at BESIII. *PoS* **2025**, QNP2024, 87. [\[CrossRef\]](#)

23. Vidaña, I. Hyperons: The strange ingredients of the nuclear equation of state. *Proc. Roy. Soc. Lond. A* **2018**, *474*, 20180145. [\[CrossRef\]](#) [\[PubMed\]](#)

24. Hiyama, E.; Nakazawa, K. Structure of $S = -2$ Hypernuclei and Hyperon–Hyperon Interactions. *Ann. Rev. Nucl. Part. Sci.* **2018**, *68*, 131–160. [\[CrossRef\]](#)

25. Tolos, L.; Fabbietti, L. Strangeness in Nuclei and Neutron Stars. *Prog. Part. Nucl. Phys.* **2020**, *112*, 103770. [\[CrossRef\]](#)

26. Lattimer, J.M.; Prakash, M. Neutron star structure and the equation of state. *Astrophys. J.* **2001**, *550*, 426–442. [\[CrossRef\]](#)

27. Lonardoni, D.; Lovato, A.; Gandolfi, S.; Pederiva, F. Hyperon Puzzle: Hints from Quantum Monte Carlo Calculations. *Phys. Rev. Lett.* **2015**, *114*, 092301. [\[CrossRef\]](#) [\[PubMed\]](#)

28. Abbott, B.P.; Abbott, R.; Abbott, T.D.; Acernese, F.; Ackley, K.; Adams, C.; Adams, T.; Addesso, P.; Adhikari, R.X.; Adya, V.B.; et al. GW170817: Measurements of neutron star radii and equation of state. *Phys. Rev. Lett.* **2018**, *121*, 161101. [\[CrossRef\]](#)

29. Ablikim, M.; Achasov, M.N.; Ai, X.C.; Albayrak, O.; Albrecht, M.; Ambrose, D.J.; Amoroso, A.; An, F.F.; An, Q.; Bai, J.Z.; et al. Design and Construction of the BESIII Detector. *Nucl. Instrum. Meth. A* **2010**, *614*, 345–399. [\[CrossRef\]](#)

30. Yu, C.; Duan, Z.; Gu, S.; Guo, Y.; Huang, X.; Ji, D.; Ji, H.; Jiao, Y.; Liu, Z.; Peng, Y.; et al. BEPCII Performance and Beam Dynamics Studies on Luminosity. In Proceedings of the 7th International Particle Accelerator Conference (IPAC2016), Busan, Republic of Korea, 8–13 May 2016; Paper TUYA01. [\[CrossRef\]](#)

31. Ablikim, M.; Achasov, M.N.; Ai, X.C.; Albayrak, O.; Albrecht, M.; Ambrose, D.J.; Amoroso, A.; An, F.F.; An, Q.; Bai, J.Z.; et al. Future Physics Programme of BESIII. *Chin. Phys. C* **2020**, *44*, 040001. [\[CrossRef\]](#)

32. Lu, J.; Xiao, Y.; Ji, X. Online monitoring of the center-of-mass energy from real data at BESIII. *Radiat. Detect. Technol. Methods* **2020**, *4*, 337–345. [\[CrossRef\]](#)

33. Zhang, J.W.; Wu, L.H.; Sun, S.S.; Zou, J.H.; Liu, C.X.; Deng, Z.Y.; Ma, Q.M.; Wen, S.P.; Cao, G.F.; Zhang, B.L.; et al. Suppression of top-up injection backgrounds with offline event filter in the BESIII experiment. *Radiat. Detect. Technol. Methods* **2022**, *6*, 289–299.

34. Li, X.; Sun, Y.J.; Li, C.; Liu, Z.; Heng, Y.K.; Shao, M.; Wang, X.Z.; Wu, Z.; Cao, P.; Chen, M.M.; et al. Study of MRPC technology for BESIII endcap-TOF upgrade. *Radiat. Detect. Technol. Methods* **2017**, *1*, 13–20. [\[CrossRef\]](#)

35. Guo, Y.X.; Sun, S.S.; An, F.F.; Yang, R.X.; Zhou, M.; Wu, Z.; Dai, H.L.; Heng, Y.K.; Li, C.; Deng, Z.Y.; et al. The study of time calibration for upgraded end cap TOF of BESIII. *Radiat. Detect. Technol. Methods* **2017**, *1*, 15–23. [\[CrossRef\]](#)

36. Cao, P.; Chen, H.F.; Chen, M.M.; Dai, H.L.; Heng, Y.K.; Ji, X.L.; Jiang, X.S.; Li, C.; Li, X.; Liu, S.B.; et al. Design and construction of the new BESIII endcap Time-of-Flight system with MRPC Technology. *Nucl. Instrum. Meth. A* **2020**, *953*, 163053. [\[CrossRef\]](#)

37. Fäldt, G. Entanglement in joint $\Lambda\bar{\Lambda}$ decay. *Eur. Phys. J. A* **2015**, *51*, 74. [\[CrossRef\]](#)

38. Fäldt, G.; Kupsc, A. Hadronic structure functions in the $e^+e^- \rightarrow \bar{\Lambda}\Lambda$ reaction. *Phys. Lett. B* **2017**, *772*, 16–21. [\[CrossRef\]](#)

39. Dubnickova, A.Z.; Dubnicka, S.; Rekalo, M.P. Investigation of the nucleon electromagnetic structure by polarization effects in $e^+e^- \rightarrow N\bar{N}$ processes. *Nuov. Cim. A* **1996**, *109*, 241–256. [\[CrossRef\]](#)

40. Tomasi-Gustafsson, E.; Lacroix, F.; Duterte, C.; Gakh, G.I. Nucleon electromagnetic form-factors and polarization observables in space-like and time-like regions. *Eur. Phys. J. A* **2005**, *24*, 419–429. [\[CrossRef\]](#)

41. Denig, A.; Salmè, G. Nucleon Electromagnetic Form Factors in the Timelike Region. *Prog. Part. Nucl. Phys.* **2013**, *68*, 113–157. [\[CrossRef\]](#)

42. Perotti, E.; Fäldt, G.; Kupsc, A.; Leupold, S.; Song, J.J. Polarization observables in e^+e^- annihilation to a baryon-antibaryon pair. *Phys. Rev. D* **2019**, *99*, 056008. [\[CrossRef\]](#)

43. Ablikim, M.; Achasov, M.N.; Ai, X.C.; Albayrak, O.; Albrecht, M.; Ambrose, D.J.; Amoroso, A.; An, F.F.; An, Q.; Bai, J.Z.; et al. Polarization and entanglement in baryon–antibaryon pair production in electron–positron annihilation. In Proceedings of the 14th International Workshop on Meson Production, Properties and Interaction (MESON 2018), Krakow, Poland, 7–12 June 2018; p. 231. [[CrossRef](#)]

44. Lee, T.D.; Yang, C.N. General Partial Wave Analysis of the Decay of a Hyperon of Spin 1/2. *Phys. Rev.* **1957**, *108*, 1645–1647. [[CrossRef](#)]

45. Donoghue, J.F.; He, X.G.; Pakvasa, S. Hyperon Decays and CP Nonconservation. *Phys. Rev. D* **1986**, *34*, 833–841. [[CrossRef](#)]

46. Donoghue, J.F.; Pakvasa, S. Signals of CP Nonconservation in Hyperon Decay. *Phys. Rev. Lett.* **1985**, *55*, 162–165. [[CrossRef](#)]

47. Ablikim, M.; Achasov, M.N.; Ai, X.C.; Albayrak, O.; Albrecht, M.; Ambrose, D.J.; Amoroso, A.; An, F.F.; An, Q.; Bai, J.Z.; et al. Precise Measurements of Decay Parameters and CP Asymmetry with Entangled $\Lambda - \bar{\Lambda}$ Pairs. *Phys. Rev. Lett.* **2022**, *129*, 131801. [[CrossRef](#)] [[PubMed](#)]

48. Ablikim, M.; Achasov, M.N.; Ai, X.C.; Albayrak, O.; Albrecht, M.; Ambrose, D.J.; Amoroso, A.; An, F.F.; An, Q.; Bai, J.Z.; et al. Extracting the femtometer structure of strange baryons using the vacuum polarization effect. *Nat. Commun.* **2024**, *15*, 8812. [[CrossRef](#)]

49. Ablikim, M.; Achasov, M.N.; Ai, X.C.; Albayrak, O.; Albrecht, M.; Ambrose, D.J.; Amoroso, A.; An, F.F.; An, Q.; Bai, J.Z.; et al. Σ^+ and $\bar{\Sigma}^-$ polarization in the J/ψ and $\psi(3686)$ decays. *Phys. Rev. Lett.* **2020**, *125*, 052004. [[CrossRef](#)]

50. Ablikim, M.; Achasov, M.N.; Ai, X.C.; Albayrak, O.; Albrecht, M.; Ambrose, D.J.; Amoroso, A.; An, F.F.; An, Q.; Bai, J.Z.; et al. Precision CP Symmetry Test and Polarization Analysis in Σ^+ Decays. *Phys. Rev. Lett.* **2025**, *135*, 141804. [[CrossRef](#)]

51. Ablikim, M.; Achasov, M.N.; Ai, X.C.; Albayrak, O.; Albrecht, M.; Ambrose, D.J.; Amoroso, A.; An, F.F.; An, Q.; Bai, J.Z.; et al. Test of CP Symmetry in Hyperon to Neutron Decays. *Phys. Rev. Lett.* **2023**, *131*, 191802. [[CrossRef](#)] [[PubMed](#)]

52. Olsen, S.; Pondrom, L.; Handler, R.; Limon, P.; Smith, J.A.; Overseth, O.E. Asymmetry parameter for $\Lambda^0 \rightarrow n\pi^0$. *Phys. Rev. Lett.* **1970**, *24*, 843–847. [[CrossRef](#)]

53. Nair, S.S.; Perotti, E.; Leupold, S. Constraining P and CP violation in the main decay of the neutral Sigma hyperon. *Phys. Lett. B* **2019**, *788*, 535–540. [[CrossRef](#)]

54. Ablikim, M.; Achasov, M.N.; Ai, X.C.; Albayrak, O.; Albrecht, M.; Ambrose, D.J.; Amoroso, A.; An, F.F.; An, Q.; Bai, J.Z.; et al. Strong and Weak CP Tests in Sequential Decays of Polarized Σ^0 Hyperons. *Phys. Rev. Lett.* **2024**, *133*, 101902. [[CrossRef](#)]

55. Ablikim, M.; Achasov, M.N.; Ai, X.C.; Albayrak, O.; Albrecht, M.; Ambrose, D.J.; Amoroso, A.; An, F.F.; An, Q.; Bai, J.Z.; et al. Tests of CP symmetry in entangled $\Xi^0 - \bar{\Xi}^0$ pairs. *Phys. Rev. D* **2023**, *108*, L031106. [[CrossRef](#)]

56. Ablikim, M.; Achasov, M.N.; Ai, X.C.; Albayrak, O.; Albrecht, M.; Ambrose, D.J.; Amoroso, A.; An, F.F.; An, Q.; Bai, J.Z.; et al. Evidence of Transverse Polarization of Ξ^0 Hyperon in $\psi(3686) \rightarrow \Xi^0 \bar{\Xi}^0$. *arXiv* **2025**, arXiv:2510.19571.

57. Ablikim, M.; Achasov, M.N.; Ai, X.C.; Albayrak, O.; Albrecht, M.; Ambrose, D.J.; Amoroso, A.; An, F.F.; An, Q.; Bai, J.Z.; et al. Probing CP symmetry and weak phases with entangled double-strange baryons. *Nature* **2022**, *606*, 64–69. [[CrossRef](#)]

58. Ablikim, M.; Achasov, M.N.; Ai, X.C.; Albayrak, O.; Albrecht, M.; Ambrose, D.J.; Amoroso, A.; An, F.F.; An, Q.; Bai, J.Z.; et al. Observation of Ξ^- hyperon transverse polarization in $\psi(3686) \rightarrow \Xi^- \bar{\Xi}^+$. *Phys. Rev. D* **2022**, *106*, L091101. [[CrossRef](#)]

59. Liu, H.; Zhang, J.; Wang, X. CP Asymmetry in the Ξ Hyperon Sector. *Symmetry* **2023**, *15*, 214. [[CrossRef](#)]

60. Ablikim, M.; Achasov, M.N.; Ai, X.C.; Albayrak, O.; Albrecht, M.; Ambrose, D.J.; Amoroso, A.; An, F.F.; An, Q.; Bai, J.Z.; et al. First simultaneous measurement of Ξ^0 and $\bar{\Xi}^0$ asymmetry parameters in $\psi(3686)$ decay. *Phys. Rev. D* **2023**, *108*, L011101. [[CrossRef](#)]

61. Ablikim, M.; Achasov, M.N.; Ai, X.C.; Albayrak, O.; Albrecht, M.; Ambrose, D.J.; Amoroso, A.; An, F.F.; An, Q.; Bai, J.Z.; et al. Investigation of the $\Delta I = 1/2$ Rule and Test of CP Symmetry through the Measurement of Decay Asymmetry Parameters in Ξ^- Decays. *Phys. Rev. Lett.* **2024**, *132*, 101801. [[CrossRef](#)]

62. Ablikim, M.; Achasov, M.N.; Ai, X.C.; Albayrak, O.; Albrecht, M.; Ambrose, D.J.; Amoroso, A.; An, F.F.; An, Q.; Bai, J.Z.; et al. Model-Independent Determination of the Spin of the Ω^- and Its Polarization Alignment in $\psi(3686) \rightarrow \Omega^- \bar{\Omega}^+$. *Phys. Rev. Lett.* **2021**, *126*, 092002. [[CrossRef](#)]

63. Doncel, M.G.; Michel, L.; Minnaert, P. Rigorous spin tests from usual strong decays. *Nucl. Phys. B* **1972**, *38*, 477–528. [[CrossRef](#)]

64. Zhang, Z.; Song, J.J.; Zhou, Y.J. Refined Analysis of $\Omega - \bar{\Omega}$ Polarization in Electron–Positron Annihilation Process. *Phys. Rev. D* **2024**, *109*, 036005. [[CrossRef](#)]

65. Ablikim, M.; Achasov, M.N.; Ai, X.C.; Albayrak, O.; Albrecht, M.; Ambrose, D.J.; Amoroso, A.; An, F.F.; An, Q.; Bai, J.Z.; et al. Measurements of the absolute branching fractions of Ω^- decays and test of the $\Delta I = 1/2$ rule. *Phys. Rev. D* **2023**, *108*, L091101. [[CrossRef](#)]

66. Wang, X.; Huang, G. Electromagnetic Form Factor of Doubly-Strange Hyperon. *Symmetry* **2022**, *14*, 65. [[CrossRef](#)]

67. Ablikim, M.; Achasov, M.N.; Ai, X.C.; Albayrak, O.; Albrecht, M.; Ambrose, D.J.; Amoroso, A.; An, F.F.; An, Q.; Bai, J.Z.; et al. Complete Measurement of the Λ Electromagnetic Form Factors. *Phys. Rev. Lett.* **2019**, *123*, 122003. [[CrossRef](#)]

68. Ablikim, M.; Achasov, M.N.; Ai, X.C.; Albayrak, O.; Albrecht, M.; Ambrose, D.J.; Amoroso, A.; An, F.F.; An, Q.; Bai, J.Z.; et al. Measurement of Λ baryon polarization in $e^+e^- \rightarrow \Lambda\bar{\Lambda}$ at $\sqrt{s} = 3.773$ GeV. *Phys. Rev. D* **2022**, *105*, L011101. [[CrossRef](#)]

69. Ablikim, M.; Achasov, M.N.; Ai, X.C.; Albayrak, O.; Albrecht, M.; Ambrose, D.J.; Amoroso, A.; An, F.F.; An, Q.; Bai, J.Z.; et al. Measurement of Λ transverse polarization in e^+e^- collisions at $\sqrt{s} = 3.68\text{--}3.71$ GeV. *J. High Energy Phys. (JHEP)* **2023**, *2023*, 81. [\[CrossRef\]](#)

70. Ablikim, M.; Achasov, M.N.; Ai, X.C.; Albayrak, O.; Albrecht, M.; Ambrose, D.J.; Amoroso, A.; An, F.F.; An, Q.; Bai, J.Z.; et al. Observation of Transverse Polarization and Determination of Electromagnetic Form Factor of Λ Hyperon at $\sqrt{s} = 3.773$ GeV. *Phys. Rev. D* **2025**, *112*, L051102. [\[CrossRef\]](#)

71. Ablikim, M.; Achasov, M.N.; Ai, X.C.; Albayrak, O.; Albrecht, M.; Ambrose, D.J.; Amoroso, A.; An, F.F.; An, Q.; Bai, J.Z.; et al. Determination of the Σ^+ Timelike Electromagnetic Form Factors. *Phys. Rev. Lett.* **2024**, *132*, 081904. [\[CrossRef\]](#)

72. Ablikim, M.; Achasov, M.N.; Ai, X.C.; Albayrak, O.; Albrecht, M.; Ambrose, D.J.; Amoroso, A.; An, F.F.; An, Q.; Bai, J.Z.; et al. Measurement of Σ^+ transverse polarization in e^+e^- collisions at $\sqrt{s} = 3.68\text{--}3.71$ GeV. *J. High Energy Phys. (JHEP)* **2024**, *2024*, 186. [\[CrossRef\]](#)

73. He, X.G.; Ma, J.P. Testing of P and CP symmetries with $e^+e^- \rightarrow J/\psi \rightarrow \Lambda\bar{\Lambda}$. *Phys. Lett. B* **2023**, *839*, 137834. [\[CrossRef\]](#)

74. Fu, J.; Li, H.-B.; Wang, J.-P.; Yu, F.-S.; Zhang, J. Probing hyperon electric dipole moments with a full angular analysis. *Phys. Rev. D* **2023**, *108*, 009000. [\[CrossRef\]](#)

75. Ablikim, M.; Achasov, M.N.; Ai, X.C.; Albayrak, O.; Albrecht, M.; Ambrose, D.J.; Amoroso, A.; An, F.F.; An, Q.; Bai, J.Z.; et al. Precise Measurement of the Λ Electric Dipole Moment through the Entangled Strange Baryon-Antibaryon System. *arXiv* **2025**, arXiv:2506.19180.

76. Behrends, R.E. Photon Decay of Hyperons. *Phys. Rev.* **1958**, *111*, 1691–1697. [\[CrossRef\]](#)

77. Hara, Y. Nonleptonic Decays of Baryons and the Eightfold Way. *Phys. Rev. Lett.* **1964**, *12*, 378–379. [\[CrossRef\]](#)

78. Gavela, M.B.; Le Yaouanc, A.; Oliver, L.; Pene, O.; Raynal, J.C.; Pham, T.N. Parity Violating Radiative Weak Decays and the Quark Model. *Phys. Lett. B* **1981**, *101*, 417–422. [\[CrossRef\]](#)

79. Nardulli, G. A Pole Model Calculation of Weak Radiative Hyperon Decays. *Phys. Lett. B* **1987**, *190*, 187–191. [\[CrossRef\]](#)

80. Zenczykowski, P. Reanalysis of weak radiative hyperon decays in combined symmetry/vector dominance approach. *Phys. Rev. D* **1991**, *44*, 1485–1490. [\[CrossRef\]](#)

81. Borasoy, B.; Holstein, B.R. Resonances in radiative hyperon decays. *Phys. Rev. D* **1999**, *59*, 054019. [\[CrossRef\]](#)

82. Zenczykowski, P. Joint description of weak radiative and nonleptonic hyperon decays in broken SU(3). *Phys. Rev. D* **2006**, *73*, 076005. [\[CrossRef\]](#)

83. Niu, P.Y.; Richard, J.M.; Wang, Q.; Zhao, Q. Hyperon Weak Radiative Decay. *Chin. Phys. C* **2021**, *45*, 013101. [\[CrossRef\]](#)

84. Shi, R.X.; Li, S.Y.; Lu, J.X.; Geng, L.S. Weak radiative hyperon decays in covariant baryon chiral perturbation theory. *Sci. Bull.* **2022**, *67*, 2298–2304. [\[CrossRef\]](#)

85. Ablikim, M.; Achasov, M.N.; Ai, X.C.; Albayrak, O.; Albrecht, M.; Ambrose, D.J.; Amoroso, A.; An, F.F.; An, Q.; Bai, J.Z.; et al. Measurement of the absolute branching fraction and decay asymmetry of $\Lambda \rightarrow n\gamma$. *Phys. Rev. Lett.* **2022**, *129*, 212002. [\[CrossRef\]](#)

86. Ablikim, M.; Achasov, M.N.; Ai, X.C.; Albayrak, O.; Albrecht, M.; Ambrose, D.J.; Amoroso, A.; An, F.F.; An, Q.; Bai, J.Z.; et al. Precision measurement of the decay $\Sigma^+ \rightarrow p\gamma$ in the process $J/\psi \rightarrow \Sigma^+\bar{\Sigma}^-$. *Phys. Rev. Lett.* **2023**, *130*, 211901. [\[CrossRef\]](#)

87. Ablikim, M.; Achasov, M.N.; Ai, X.C.; Albayrak, O.; Albrecht, M.; Ambrose, D.J.; Amoroso, A.; An, F.F.; An, Q.; Bai, J.Z.; et al. Measurement of the decay $\Xi^0 \rightarrow \Lambda\gamma$ with entangled $\Xi^0\bar{\Xi}^0$ pairs. *Sci. Bull.* **2025**, *70*, 454–459. [\[CrossRef\]](#)

88. Navas, S.; Amsler, C.; Gutsche, T.; Hanhart, C.; Hernández-Rey, J.J.; Lourenço, C.; Masoni, A.; Mikhasenko, M.; Mitchell, R.E.; Patrignani, C.; et al. Review of particle physics. *Phys. Rev. D* **2024**, *110*, 030001. [\[CrossRef\]](#)

89. Ablikim, M.; Achasov, M.N.; Ai, X.C.; Albayrak, O.; Albrecht, M.; Ambrose, D.J.; Amoroso, A.; An, F.F.; An, Q.; Bai, J.Z.; et al. Search for baryon and lepton number violating decays of Ξ^0 hyperons. *Phys. Rev. D* **2023**, *108*, 012006. [\[CrossRef\]](#)

90. Ablikim, M.; Achasov, M.N.; Ai, X.C.; Albayrak, O.; Albrecht, M.; Ambrose, D.J.; Amoroso, A.; An, F.F.; An, Q.; Bai, J.Z.; et al. First Measurement of the Absolute Branching Fraction of $\Lambda \rightarrow p\mu^-\bar{\nu}_\mu$. *Phys. Rev. Lett.* **2021**, *127*, 121802. [\[CrossRef\]](#)

91. Ablikim, M.; Achasov, M.N.; Ai, X.C.; Albayrak, O.; Albrecht, M.; Ambrose, D.J.; Amoroso, A.; An, F.F.; An, Q.; Bai, J.Z.; et al. Search for the hyperon semileptonic decay $\Xi^- \rightarrow \Xi^0 e^- \bar{\nu}_e$. *Phys. Rev. D* **2021**, *104*, 072007. [\[CrossRef\]](#)

92. Ablikim, M.; Achasov, M.N.; Ai, X.C.; Albayrak, O.; Albrecht, M.; Ambrose, D.J.; Amoroso, A.; An, F.F.; An, Q.; Bai, J.Z.; et al. Search for hyperon $\Delta S = \Delta Q$ violating decay $\Xi^0 \rightarrow \Sigma^- e^+ \nu_e$. *Phys. Rev. D* **2023**, *107*, 012002. [\[CrossRef\]](#)

93. Bifani, S.; Descotes-Genon, S.; Romero Vidal, A.; Schune, M.H. Review of Lepton Universality tests in B decays. *J. Phys. G* **2019**, *46*, 023001. [\[CrossRef\]](#)

94. Chang, H.M.; González-Alonso, M.; Martin Camalich, J. Nonstandard Semileptonic Hyperon Decays. *Phys. Rev. Lett.* **2015**, *114*, 161802. [\[CrossRef\]](#)

95. Ablikim, M.; Achasov, M.N.; Ai, X.C.; Albayrak, O.; Albrecht, M.; Ambrose, D.J.; Amoroso, A.; An, F.F.; An, Q.; Bai, J.Z.; et al. Measurement of the proton form factor by studying $e^+e^- \rightarrow p\bar{p}$. *Phys. Rev. D* **2015**, *91*, 112004. [\[CrossRef\]](#)

96. Ablikim, M.; Achasov, M.N.; Ai, X.C.; Albayrak, O.; Albrecht, M.; Ambrose, D.J.; Amoroso, A.; An, F.F.; An, Q.; Bai, J.Z.; et al. Study of the process $e^+e^- \rightarrow p\bar{p}$ via initial state radiation at BESIII. *Phys. Rev. D* **2019**, *99*, 092002. [\[CrossRef\]](#)

97. Ablikim, M.; Achasov, M.N.; Ai, X.C.; Albayrak, O.; Albrecht, M.; Ambrose, D.J.; Amoroso, A.; An, F.F.; An, Q.; Bai, J.Z.; et al. Measurement of proton electromagnetic form factors in $e^+e^- \rightarrow p\bar{p}$ in the energy region 2.00–3.08 GeV. *Phys. Rev. Lett.* **2020**, *124*, 042001. [\[CrossRef\]](#)

98. Ablikim, M.; Achasov, M.N.; Ai, X.C.; Albayrak, O.; Albrecht, M.; Ambrose, D.J.; Amoroso, A.; An, F.F.; An, Q.; Bai, J.Z.; et al. Oscillating features in the electromagnetic structure of the neutron. *Nat. Phys.* **2021**, *17*, 1200. [\[CrossRef\]](#)

99. Ablikim, M.; Achasov, M.N.; Ai, X.C.; Albayrak, O.; Albrecht, M.; Ambrose, D.J.; Amoroso, A.; An, F.F.; An, Q.; Bai, J.Z.; et al. Observation of a cross-section enhancement near mass threshold in $e^+e^- \rightarrow \Lambda\bar{\Lambda}$. *Phys. Rev. D* **2018**, *97*, 032013. [\[CrossRef\]](#)

100. Ablikim, M.; Achasov, M.N.; Ai, X.C.; Albayrak, O.; Albrecht, M.; Ambrose, D.J.; Amoroso, A.; An, F.F.; An, Q.; Bai, J.Z.; et al. Measurement of the $e^+e^- \rightarrow \Lambda\bar{\Sigma}^0 + \text{c.c.}$ cross sections at \sqrt{s} from 2.3094 to 3.0800 GeV. *Phys. Rev. D* **2024**, *109*, 012002. [\[CrossRef\]](#)

101. Ablikim, M.; Achasov, M.N.; Ai, X.C.; Albayrak, O.; Albrecht, M.; Ambrose, D.J.; Amoroso, A.; An, F.F.; An, Q.; Bai, J.Z.; et al. Measurements of Σ^+ and Σ^- time-like electromagnetic form factors for center-of-mass energies from 2.3864 to 3.0200 GeV. *Phys. Lett. B* **2021**, *814*, 136110. [\[CrossRef\]](#)

102. Ablikim, M.; Achasov, M.N.; Ai, X.C.; Albayrak, O.; Albrecht, M.; Ambrose, D.J.; Amoroso, A.; An, F.F.; An, Q.; Bai, J.Z.; et al. Measurement of the $e^+e^- \rightarrow \Sigma^0\bar{\Sigma}^0$ cross sections at center-of-mass energies from 2.3864 to 3.0200 GeV. *Phys. Lett. B* **2022**, *831*, 137187. [\[CrossRef\]](#)

103. Ablikim, M.; Achasov, M.N.; Ai, X.C.; Albayrak, O.; Albrecht, M.; Ambrose, D.J.; Amoroso, A.; An, F.F.; An, Q.; Bai, J.Z.; et al. Measurement of cross section for $e^+e^- \rightarrow \Xi^-\bar{\Xi}^+$ near threshold at BESIII. *Phys. Rev. D* **2021**, *103*, 012005. [\[CrossRef\]](#)

104. Ablikim, M.; Achasov, M.N.; Ai, X.C.; Albayrak, O.; Albrecht, M.; Ambrose, D.J.; Amoroso, A.; An, F.F.; An, Q.; Bai, J.Z.; et al. Measurement of cross section for $e^+e^- \rightarrow \Xi^0\bar{\Xi}^0$ near threshold. *Phys. Lett. B* **2021**, *820*, 136557. [\[CrossRef\]](#)

105. Ablikim, M.; Achasov, M.N.; Ai, X.C.; Albayrak, O.; Albrecht, M.; Ambrose, D.J.; Amoroso, A.; An, F.F.; An, Q.; Bai, J.Z.; et al. Study of $e^+e^- \rightarrow \Omega^-\bar{\Omega}^+$ at center-of-mass energies from 3.49 to 3.67 GeV. *Phys. Rev. D* **2023**, *107*, 052003. [\[CrossRef\]](#)

106. Ablikim, M.; Achasov, M.N.; Ai, X.C.; Albayrak, O.; Albrecht, M.; Ambrose, D.J.; Amoroso, A.; An, F.F.; An, Q.; Bai, J.Z.; et al. Measurement of the cross section for $e^+e^- \rightarrow \Xi^-\bar{\Xi}^+$ and observation of an excited Ξ baryon. *Phys. Rev. Lett.* **2020**, *124*, 032002. [\[CrossRef\]](#)

107. Ablikim, M.; Achasov, M.N.; Ai, X.C.; Albayrak, O.; Albrecht, M.; Ambrose, D.J.; Amoroso, A.; An, F.F.; An, Q.; Bai, J.Z.; et al. Measurement of the cross section for $e^+e^- \rightarrow \Lambda\bar{\Lambda}$ and evidence of the decay $\psi(3770) \rightarrow \Lambda\bar{\Lambda}$. *Phys. Rev. D* **2021**, *104*, L091104. [\[CrossRef\]](#)

108. Ablikim, M.; Achasov, M.N.; Ai, X.C.; Albayrak, O.; Albrecht, M.; Ambrose, D.J.; Amoroso, A.; An, F.F.; An, Q.; Bai, J.Z.; et al. Measurement of Born cross section of $e^+e^- \rightarrow \Sigma^+\bar{\Sigma}^-$ at center-of-mass energies between 3.510 and 4.951 GeV. *J. High Energy Phys. (JHEP)* **2024**, *2024*, 22. [\[CrossRef\]](#)

109. Ablikim, M.; Achasov, M.N.; Ai, X.C.; Albayrak, O.; Albrecht, M.; Ambrose, D.J.; Amoroso, A.; An, F.F.; An, Q.; Bai, J.Z.; et al. Measurement of Born cross section of $e^+e^- \rightarrow \Sigma^0\bar{\Sigma}^0$ at $\sqrt{s} = 3.50\text{--}4.95$ GeV. *Phys. Rev. D* **2025**, *111*, L051502. [\[CrossRef\]](#)

110. Ablikim, M.; Achasov, M.N.; Ai, X.C.; Albayrak, O.; Albrecht, M.; Ambrose, D.J.; Amoroso, A.; An, F.F.; An, Q.; Bai, J.Z.; et al. Measurement of Born cross sections of $e^+e^- \rightarrow \Xi^0\bar{\Xi}^0$ and search for charmonium(-like) states at $\sqrt{s} = 3.51\text{--}4.95$ GeV. *J. High Energy Phys. (JHEP)* **2024**, *2024*, 62. [\[CrossRef\]](#)

111. Ablikim, M.; Achasov, M.N.; Ai, X.C.; Albayrak, O.; Albrecht, M.; Ambrose, D.J.; Amoroso, A.; An, F.F.; An, Q.; Bai, J.Z.; et al. Measurement of Born cross sections and effective form factors of $e^+e^- \rightarrow \Omega^-\bar{\Omega}^+$ from $\sqrt{s} = 3.7$ to 4.7 GeV. *arXiv* **2025**, arXiv:2508.01359.

112. Zhang, R.; Wang, X. Search for charmonium(-like) states decaying into the $\Omega^-\bar{\Omega}^+$ final states. *arXiv* **2025**, arXiv:2508.03454.

113. Ablikim, M.; Achasov, M.N.; Ai, X.C.; Albayrak, O.; Albrecht, M.; Ambrose, D.J.; Amoroso, A.; An, F.F.; An, Q.; Bai, J.Z.; et al. Measurement of the cross section of $e^+e^- \rightarrow \Xi^-\bar{\Xi}^+$ at center-of-mass energies between 3.510 and 4.843 GeV. *J. High Energy Phys. (JHEP)* **2023**, *2023*, 228. [\[CrossRef\]](#)

114. Ablikim, M.; Achasov, M.N.; Ai, X.C.; Albayrak, O.; Albrecht, M.; Ambrose, D.J.; Amoroso, A.; An, F.F.; An, Q.; Bai, J.Z.; et al. Measurement of the cross sections of $e^+e^- \rightarrow K^-\bar{\Xi}^+\Lambda/\Sigma^0$ at center-of-mass energies between 3.510 and 4.914 GeV. *J. High Energy Phys. (JHEP)* **2024**, *2024*, 258. [\[CrossRef\]](#)

115. Ablikim, M.; Achasov, M.N.; Ai, X.C.; Albayrak, O.; Albrecht, M.; Ambrose, D.J.; Amoroso, A.; An, F.F.; An, Q.; Bai, J.Z.; et al. Observation of a near-threshold enhancement in the $\Lambda\bar{\Lambda}$ mass spectrum from $e^+e^- \rightarrow \phi\Lambda\bar{\Lambda}$ at \sqrt{s} from 3.51 to 4.60 GeV. *Phys. Rev. D* **2021**, *104*, 052006. [\[CrossRef\]](#)

116. Ablikim, M.; Achasov, M.N.; Ai, X.C.; Albayrak, O.; Albrecht, M.; Ambrose, D.J.; Amoroso, A.; An, F.F.; An, Q.; Bai, J.Z.; et al. Measurement of $e^+e^- \rightarrow pK^-\bar{\Lambda} + \text{c.c.}$ cross sections between 4.009 GeV and 4.951 GeV. *J. High Energy Phys. (JHEP)* **2023**, *2023*, 27. [\[CrossRef\]](#)

117. Ablikim, M.; Achasov, M.N.; Ai, X.C.; Albayrak, O.; Albrecht, M.; Ambrose, D.J.; Amoroso, A.; An, F.F.; An, Q.; Bai, J.Z.; et al. Measurement of $e^+e^- \rightarrow \Lambda\bar{\Lambda}\eta$ from 3.5106 to 4.6988 GeV and study of $\Lambda\bar{\Lambda}$ mass threshold enhancement. *Phys. Rev. D* **2023**, *107*, 112001. [\[CrossRef\]](#)

118. Ablikim, M.; Achasov, M.N.; Ai, X.C.; Albayrak, O.; Albrecht, M.; Ambrose, D.J.; Amoroso, A.; An, F.F.; An, Q.; Bai, J.Z.; et al. Determination of spin-parity quantum numbers for the narrow structure near the $p\bar{\Lambda}$ threshold in $e^+e^- \rightarrow pK^-\bar{\Lambda} + \text{c.c.}$ *Phys. Rev. Lett.* **2023**, *131*, 151901. [[CrossRef](#)]

119. Ablikim, M.; Achasov, M.N.; Ai, X.C.; Albayrak, O.; Albrecht, M.; Ambrose, D.J.; Amoroso, A.; An, F.F.; An, Q.; Bai, J.Z.; et al. Study of $e^+e^- \rightarrow 2(p\bar{p})$ at center-of-mass energies between 4.0 and 4.6 GeV. *Phys. Rev. D* **2021**, *103*, 052003. [[CrossRef](#)]

120. Ablikim, M.; Achasov, M.N.; Ai, X.C.; Albayrak, O.; Albrecht, M.; Ambrose, D.J.; Amoroso, A.; An, F.F.; An, Q.; Bai, J.Z.; et al. Observation of $e^+e^- \rightarrow ppp\bar{n}\pi^- + \text{c.c.}$ *Chin. Phys. C* **2023**, *47*, 043001. [[CrossRef](#)]

121. Ablikim, M.; Achasov, M.N.; Ai, X.C.; Albayrak, O.; Albrecht, M.; Ambrose, D.J.; Amoroso, A.; An, F.F.; An, Q.; Bai, J.Z.; et al. Search for the production of deuterons and antideuterons in e^+e^- annihilation at center-of-mass energies between 4.13 and 4.70 GeV. *Phys. Rev. D* **2024**, *109*, 092013. [[CrossRef](#)]

122. Ablikim, M.; Achasov, M.N.; Ai, X.C.; Albayrak, O.; Albrecht, M.; Ambrose, D.J.; Amoroso, A.; An, F.F.; An, Q.; Bai, J.Z.; et al. Measurement of the Born cross section for $e^+e^- \rightarrow pK^-K^-\Xi^+$ at $\sqrt{s} = 3.5\text{--}4.9$ GeV. *J. High Energy Phys. (JHEP)* **2025**, *2025*, 111. [[CrossRef](#)]

123. Yuan, C.Z.; Karliner, M. Cornucopia of antineutrons and hyperons from a super J/ψ factory for next-generation nuclear and particle physics high-precision experiments. *Phys. Rev. Lett.* **2021**, *127*, 012003. [[CrossRef](#)]

124. Dai, J.; Li, H.B.; Miao, H.; Zhang, J. Prospects to study hyperon-nucleon interactions at BESIII. *Chin. Phys. C* **2024**, *48*, 073003. [[CrossRef](#)]

125. Ablikim, M.; Achasov, M.N.; Ai, X.C.; Albayrak, O.; Albrecht, M.; Ambrose, D.J.; Amoroso, A.; An, F.F.; An, Q.; Bai, J.Z.; et al. First study of reaction $\Xi^0n \rightarrow \Xi^-p$ using Ξ^0 -nucleus scattering at an electron-positron collider. *Phys. Rev. Lett.* **2023**, *130*, 251902. [[CrossRef](#)]

126. Ablikim, M.; Achasov, M.N.; Ai, X.C.; Albayrak, O.; Albrecht, M.; Ambrose, D.J.; Amoroso, A.; An, F.F.; An, Q.; Bai, J.Z.; et al. First measurement of ΛN inelastic scattering with Λ from $e^+e^- \rightarrow J/\psi \rightarrow \Lambda\bar{\Lambda}$. *Phys. Rev. C* **2024**, *109*, L052201. [[CrossRef](#)]

127. Ablikim, M.; Achasov, M.N.; Ai, X.C.; Albayrak, O.; Albrecht, M.; Ambrose, D.J.; Amoroso, A.; An, F.F.; An, Q.; Bai, J.Z.; et al. First study of antihyperon-nucleon scattering $\bar{\Lambda}p \rightarrow \bar{\Lambda}p$ and measurement of $\Lambda p \rightarrow \Lambda p$ cross section. *Phys. Rev. Lett.* **2024**, *132*, 231902. [[CrossRef](#)]

128. Wang, X.Y.; Gao, Y.; Liu, X. Understanding of the BESIII measurement of (anti)hyperon-nucleon scattering. *Phys. Lett. B* **2025**, *862*, 139321. [[CrossRef](#)]

129. Ablikim, M.; Achasov, M.N.; Ai, X.C.; Albayrak, O.; Albrecht, M.; Ambrose, D.J.; Amoroso, A.; An, F.F.; An, Q.; Bai, J.Z.; et al. First measurement of $\Sigma^+n \rightarrow \Lambda p$ and $\Sigma^+n \rightarrow \Sigma^0p$ cross-sections via Σ^+ -nucleus scattering at an electron-positron collider. *arXiv* **2025**, arXiv:2505.19907.

Disclaimer/Publisher's Note: The statements, opinions and data contained in all publications are solely those of the individual author(s) and contributor(s) and not of MDPI and/or the editor(s). MDPI and/or the editor(s) disclaim responsibility for any injury to people or property resulting from any ideas, methods, instructions or products referred to in the content.